Published OnlineFirst March 12, 2019; DOI: 10.1158/1078-0432.CCR-18-3033

Translational Cancer Mechanisms and Therapy

Clinical Cancer Research

PAK Kinase Inhibition Has Therapeutic Activity in Novel Preclinical Models of Adult T-Cell Leukemia/Lymphoma

Elaine Y. Chung[1], Yun Mai[1], Urvi A. Shah[2], Yongqiang Wei[1,3], Elise Ishida[1], Keisuke Kataoka[4], Xiaoxin Ren[5], Kith Pradhan[6], Boris Bartholdy[1], Xiaolei Wei[1,3], Yiyu Zou[2], Jinghang Zhang[5], Seishi Ogawa[7], Ulrich Steidl[1], Xingxing Zang[5], Amit Verma[2,5], Murali Janakiram[2], and B. Hilda Ye[1]

Abstract

Purpose: To evaluate therapeutic activity of PAK inhibition in ATLL and to characterize the role of PAK isoforms in cell proliferation, survival, and adhesion of ATLL cells in preclinical models.

Experimental Design: Frequency and prognostic impact of *PAK2* amplification were evaluated in an ATLL cohort of 370 cases. Novel long-term cultures and *in vivo* xenograft models were developed using primary ATLL cells from North American patients. Two PAK inhibitors were used to block PAK kinase activity pharmacologically. siRNA-based gene silencing approach was used to genetically knockdown (KD) PAK1 and PAK2 in ATLL cell lines.

Results: PAK1/2/4 are the three most abundantly expressed PAK family members in ATLL. *PAK2* amplifications are seen in 24% of ATLLs and are associated with worse prognosis in a large patient cohort. The pan-PAK inhibitor PF-3758309 (PF) has strong *in vitro* and *in vivo* activity in a variety of ATLL preclinical models. These activities of PF are likely attributed to its ability to target several PAK isoforms simultaneously because genetic silencing of either PAK1 or PAK2 produced more modest effects. PAK2 plays a major role in CADM1-mediated stromal interaction, which is an important step in systemic dissemination of the disease. This finding is consistent with the observation that *PAK2* amplification is more frequent in aggressive ATLLs and correlates with inferior outcome.

Conclusions: PAK2, a gene frequently amplified in ATLL, facilitates CADM1-mediated stromal interaction and promotes survival of ATLL cells. Taken together, PAK inhibition may hold significant promise as a targeted therapy for aggressive ATLLs.

Introduction

Adult T-cell Leukemia/Lymphoma (ATLL) is a highly aggressive T-cell neoplasm caused by human T-cell lymphotropic virus (HTLV)-1 (1, 2). Patients diagnosed with the aggressive subtypes carry some of the worst prognosis of any of the non-Hodgkin lymphomas. The 5-year overall survival (OS) rate of patients with ATLL is reported to be only 14% (3). In accordance with the endemic regions of HTLV-1, ATLL is most frequently diagnosed in southwest Japan and the Caribbean islands. Most patients with ATLL diagnosed in North American (NA-ATLL) are of Caribbean descent. Compared with the Japanese patients (J-ATLL), NA-ATLLs tend to have a more aggressive clinical course, higher rates of chemo-refractory disease, and worse prognosis (4–6). Such differences in clinical behavior may be accounted for by distinct somatic mutation patterns between these two patient populations (7). Although there is no standard therapy for ATLL, the initial treatment often employs combination chemotherapy followed by allogeneic transplantation (1). Yet, the high rate of chemo-resistance disease often leads to treatment failure and dismal survival outcomes. Hence, an attractive strategy is to design mechanism-based treatment that could target novel pathways critical in maintaining ATLL phenotype *in vivo*.

The current model for ATLL pathogenesis depicts the initial infection of CD4 T cells by HTLV-1, followed by downregulation of the HTLV-1 Tax protein, and progressive accumulation of genetic and epigenetic changes in the infected T cells that ultimately lead to oncogenic transformation and disease progression (2). In an integrated genomics and transcriptomics study of a large cohort of 426 J-ATLL patients, many frequently altered genes encoding candidate driver mutations in ATLL transformation and progression were reported (8). These genes are involved in the TCR/NF-κB signaling, T-cell trafficking, and immune surveillance. Among the 35 genes frequently targeted by both somatic alterations and the HTLV-1 onco-protein Tax, p21-activated kinase (PAK) 2 is amplified in 24% of the cases (8). PAKs are a family of serine/threonine kinases composed of six isoforms (PAK1-6).

[1]Department of Cell Biology, Albert Einstein College of Medicine, Bronx, New York. [2]Department of Oncology, Montefiore Medical Center, Bronx, New York. [3]Department of Hematology, Nanfang Hospital, Southern Medical University, Guangzhou, China. [4]Division of Molecular Oncology, National Cancer Center Research Institute, Tokyo, Japan. [5]Department of Microbiology & Immunology, Albert Einstein College of Medicine, Bronx, New York. [6]Department of Developmental and Molecular Biology, Albert Einstein College of Medicine, Bronx, New York. [7]Department of Pathology and Tumor Biology, Kyoto University, Kyoto, Japan.

Note: Supplementary data for this article are available at Clinical Cancer Research Online (http://clincancerres.aacrjournals.org/).

Corresponding Author: Bihui Hilda Ye, Albert Einstein College of Medicine, 1300 Morris Park Avenue, Bronx, NY 10461. Phone: 718-430-3339; Fax: 718-430-8574; E-mail: hilda.ye@einstein.yu.edu

Clin Cancer Res 2019;25:3589–601

doi: 10.1158/1078-0432.CCR-18-3033

Published OnlineFirst March 12, 2019; DOI: 10.1158/1078-0432.CCR-18-3033

Translational Relevance

Adult T-cell leukemia/lymphoma (ATLL) is a rare but extremely aggressive cancer, associated with a dismal outcome and lack of effective therapies. Analysis of a large cohort of ATLL samples shows 24% of patients with ATLL carry amplification of the p21-activated kinase (PAK) 2 gene and the amplification is associated with a worse prognosis. Functional studies show that the PAK kinase inhibitor PF-3758309 has profound anti-ATLL activity in *in vitro* and newly established xenograft models of this disease. We further show by siRNA-mediated gene knockdown approach that PAK2 but not PAK1 is an important regulator of heterophilic cell–cell interaction between ATLL cells and lymph node stromal cells, thus implicating PAK2 as a critical player in ATLL disease dissemination. In summary, these data suggest that PAK2 is an important driver of systemic disease in ATLL and that targeting PAK kinases may be of therapeutic benefit for this fatal malignancy.

These isoforms are separated into two groups. Group I PAKs (PAK1/2/3) are activated by signals emanating from the small GTPase CDC42 or RAC, whereas group II PAKs (PAK4/5/6) are only activated by CDC42 (9). In solid tumors, PAKs are frequently upregulated and/or hyper-activated either as the consequence of gene amplification (PAK1/4) or more so by changes in upstream regulators (8, 10). PAKs influence cancer cell proliferation and survival through a number of downstream signaling pathways, which often feed into the nuclear transcription program. Among these, the ones most relevant to ATLL biology are TCR/NF-κB, STAT5, ERK, β-catenin, and Raf/BAD (8). PAKs can also regulate cancer cell migration and metastasis through their cytoplasmic substrates involved in cytoskeletal remodeling, for example, PAK1/2 can modulate Rac GTP activity and lamellipodia formation (9).

In the ATLL microenvironment, migrating leukemic cells rely on lamellipodia formation at the leading edge to bind to and spread on stromal cells (11). Previous studies have shown that this process involves the ectopically expressed adhesion molecule CADM1/TSLC1 (11, 12), and is a key step in organ infiltration of ATLL cells in animal models (13). In patients with ATLL , CADM1 expression in combination with CD7 downregulation closely correlates with clonal expansion of leukemic cells (14). Functionally, trans-homophilic interactions of CADM1 activates PI3K (15) and NF-κB (16), whereas trans-heterophilic CADM1 interaction triggers recruitment of the RAC1 GEF, TIAM1, to the CADM1-cytoplasmic domain, leading to RAC1 activation and remodeling of actin-network and lamellipodia formation (11). Although RAC1 is known to be required for CADM1 function in ATLL, PAK kinases supporting CADM1-dependent stroma adhesion of ATLL cells have not been defined.

Because cancers with aberrantly activated PAKs are often addicted to their activity (9) and PAK signaling can drive acquired drug resistance to targeted therapies in several types of cancers (17–20), the PAK family kinases have been explored as therapeutic targets in a number of solid tumors and hematologic malignancies (18, 19, 21, 22). In this study, we evaluated the therapeutic value of PAK inhibition in ATLL preclinical models. We also examined the role of PAK1 and PAK2 in ATLL cell proliferation, survival, and stroma adhesion.

Materials and Methods

Additional methods and details are described in Supplementary Materials and Methods, available online at the CCR Web site.

Cell cultures

Su9T01, ED40515(+), ED40515(−), ED41214(+), ED41214(−), ATL55T(+), ATL43T(+), and ATL43Tb(−) were J-ATLL cell lines. ATL13, ATL18, and ATL21 were long-term $CD4^+$ T-cell cultures derived from NA-ATLL patients (Supplementary Fig. S1; ref. 7). ED40515(+), ED41214(+), ATL55T(+), ATL43T(+) cells, and the NA-ATLL cell lines were grown in the presence of 100 unit/mL human IL2. All J-ATLL cell lines, the five HTLV-1-negative human T cell lines (Jurkat, CEM, HuT78, MAC1, OCI-Ly13.2), and the human follicular dendritic cell (FDC) cell line, HK (23), were cultured in RPMI with 10% FBS. Two additional HTLV-1-negative T cell lines HH and FePD1 were maintained in IMDM and DMEM containing 20% FBS, respectively. All NA-ATLL cell lines and short-term cultures were maintained in IMDM containing 20% human serum. All medium were supplemented with 100 unit/mL penicillin and 100 μg/mL streptomycin. All cell cultures has been routinely tested for mycoplasma contamination.

In vitro cytotoxicity assay

PF-3758309 (PF, Selleckchem; Catalog No. S7094) is an ATP-competitive inhibitor that targets PAK1, PAK2, PAK3, and PAK4. IPA-3 (Tocris; Catalog No. 3622) is a selective non-ATP competitive PAK1 inhibitor that also binds PAK2 and PAK3. The IC_{50} of PF-3758309 and IPA3 were determined using resazurin (R&D Systems; Catalog No. AR002)-based viability assays in which cells were exposed to various concentrations of the reagents for 48 hours. To evaluate the response to IPA-3, a structurally related inactive compound, PIR3.5 (Tocris; Catalog No. 4212), was also tested.

Adhesion assay

A total of 7×10^3 HK cells/well were seeded in a 96-well plate and allowed to attach overnight before the assay. Parental ATLL cells or ATLL cells that were transfected with siRNA oligos 48 hours earlier were fluorescently labeled with the Calcein AM dye according to the manufacturer's instructions (Invitrogen; Catalog No. C3100MP). Labeled parental ATLL cells were then treated with either DMSO or PF at 2.5 μmol/L for 1 hour prior to exposure to HK. Subsequently, ATLL cells were added to the HK feeder-coated 96-well plate in triplicate at 7×10^4 cells/well and allowed to adhere for 180, 150, 120, 90, 30, and 15 minutes. Non-attached cells were washed away four times with 1x PBS. Absorbance reading was performed at 480 to 520 nm with the Fluostar plate reader. Adherence of ATLL cells to HK feeder was calculated as the fraction A/B. A is the absorbance values after washing away unattached cells minus average absorbance values of HK cells alone after washing. B is the absorbance values of cells before washing minus average absorbance values of HK cells alone before washing.

Xenograft studies of *in vivo* PF-3758309 activity

A patient-derived xenograft (PDX) model was established from patient PBMCs (ATL18) in NSG (NOD/SCID/γC-/-) mice by serially passaging subcutaneous tumor mass in female NSG mice. In this model, distal dissemination is a constant feature that

Published OnlineFirst March 12, 2019; DOI: 10.1158/1078-0432.CCR-18-3033

always involves lung, liver, and spleen whereas kidney and bone marrow are less frequently infiltrated. A cell line-derived xenograft (CDX) model was similarly developed using ATL43Tb(−) cells but metastasis in this model is largely restricted to the lung. PF treatment was initiated when tumors reached ∼100 mm (3). Animals were randomly assigned to one of the three groups to be treated by vehicle, 6 or 12 mg/kg/day of PF. PF was formulated in 2% carboxymethyl cellulose (24) and administered intraperitoneally. Throughout the experiment, overall health of the animals was closely monitored, body weight and tumor growth were frequently recorded. Tumor sizes were measured using an electronic caliper. Tumor volume (mm^3) was calculated using the formula of $(A \times B^2)/2$, where A and B are the tumor length and width in mm, respectively. Tumor growth inhibition (TGI) was calculated as TGI (%) $= (V_c - V_t)/(V_c - V_0) \times 100$, where V_c, V_t are the median tumor volume of control and treated groups at the end of the study and V_0 is the median tumor volume at the start of the study. All mice were maintained and treated in compliance with IACUC approved protocols at Albert Einstein College of Medicine.

Results

Amplification of *PAK2* is a frequent event in ATLL and correlates with inferior survival

Copy number variation in a cohort of 426 Japanese ATLL samples was studied using SNP array karyotyping (8). Among the 26 focally amplified region is a band on 3q29, encoding *PAK2* (Supplementary Fig. S2A). In all, *PAK2* amplification was detected in 24.4% of all ATLL cases with a preferential enrichment in the aggressive subtypes (acute/lymphomatous vs. chronic/smoldering: 27.5% vs. 16.0%; Benjamini–Hochberg correction, $q = 0.09$). There is a trend for increased *PAK2* mRNA expression in 3q29 amplified cases (Supplementary Fig. S2B) Most importantly, *PAK2* amplification was significantly associated with a trend for poor overall survival ($P = 0.029$, Fig. 1A).

Expression patterns of PAK family members in ATLL

Given *PAK2* amplification in ATLL, we wanted to examine expression pattern of this kinase in primary samples. We first established mRNA expression profiles for all six PAK family members in this disease. In acute ATLL, a significant fraction of peripheral blood mononuclear cells (PBMC) are leukemic T cells. We therefore performed qRT-PCR assays for *PAK1-6* on 6 PBMC samples from patients with ATLL and compared them to four healthy controls (Fig. 1B). *PAK2* is expressed at the highest levels among all samples followed by *PAK1*. Ranking third, *PAK4* mRNA level is approximately one log lower than *PAK1* but still approximately one log higher than *PAK3* and *PAK6*. *PAK5* mRNA is undetectable in most patient samples. The same pattern is observed from the RNA-seq dataset of the Japanese ATLL cohort (Supplementary Fig. S2C).

To measure *PAK* mRNA expression in pure populations of ATLL cells, we then analyzed eight ATLL cell lines and compared the results to normal resting and activated $CD4^+$ T cells, a pooled normal Treg sample, and four cell lines representing other T-cell non-Hodgkin lymphomas (Jurkat and CEM, acute lymphocytic leukemia; HuT78, cutaneous T-cell lymphoma; OCI-Ly13.2, peripheral T-cell lymphoma; Fig. 1C). The pattern for *PAK* isoforms among ATLL cell lines largely resembles that seen with patient PBMCs, although *PAK3* and *PAK6* mRNAs exhibit much more intragroup heterogeneity. Compared with normal resting CD4 T cells, ATLL cell lines under-express several PAK isoforms including *PAK1*, *PAK2*, *PAK4*, and *PAK6*. The same trend exists in another ATLL gene expression dataset (Supplementary Fig. S2D; ref. 25). Of note, when compared with activated CD4 T cells and other types of T-cell malignancies, *PAK2* mRNA is also reduced in ATLL cell lines (Fig. 1C). In general, Tregs have the lowest levels of all *PAKs* among all tested samples except for *PAK2*, which is expressed at comparable levels in Tregs and ATLL cell lines. Although the cause of this apparent ATLL-associated *PAK2* down-regulation is currently unknown, the observation does suggest that the level of PAK2 may have become rate-limiting in this disease and thus gene amplification events are positively selected in aggressive ATLLs. This interpretation is in line with observations made on PAK1/2 proteins. Western blot analysis shows significant variability of PAK1 protein across all diagnostic categories of T-cell malignancies, whereas PAK2 protein exhibits less variability across the panel (Fig. 1D). It should be noted that the characteristic ATLL-associated reduction of *PAK2* mRNA is not reflected at the protein level. We interpreted this result as a suggestion that posttranscriptional mechanisms such as protein stability may operate to compensate for the reduced *PAK2* mRNA expression. In summary, our result indicates that *PAK1/2/4* are the most abundantly expressed PAK isoforms in ATLL and that *PAK2* is regulated differently from the other *PAK*s during ATLL development.

PAK inhibitors have *in vitro* activity against primary ATLL samples and ATLL cell lines

Given the PAK family expression patterns in ATLL, we selected two PAK inhibitors for pharmacologic PAK inhibition. PF-3758309 (PF) is the first PAK inhibitor to advance to clinical trial. It is an ATP-competitive inhibitor with documented activity against all PAK family members to various degree (26, 27). IPA-3 is an allosteric inhibitor that has specific activity against group I PAKs but spares group II PAKs (28). In all, seven J-ATLL cell lines, seven North American patient samples, and three NA-ATLL cell lines were tested (Fig. 2A–C; Supplementary Fig. S3). For PF, the 48 hours IC_{50} values range from 1.8 to 13.4 μmol/L for the seven Japanese cell lines tested. IL2 requirement culture condition did not appear to impact PF sensitivity. For NA-ATLLs, the IC_{50} values range from 1.2 to 14.4 μmol/L for the seven primary patient samples and 2.9 to 8.2 μmol/L for the three cell lines. Of note, ATL6a/6b/6c and ATL19a/19b are serial samples collected from chemo-refractory patients treated with high-dose chemotherapy in combination with antiviral agents. We also tested IPA-3 responsiveness in six Japanese cell lines and two North American ATLL samples. Relatively low IC_{50}s were observed (6.6–16.9 μmol/L), demonstrating *in vitro* efficacy of both pharmacologic inhibitors in both Japanese and North American ATLLs (Fig. 2C; Supplementary Fig. S3C and S3D). Interestingly, activated normal CD4 T cells are highly sensitive to PF ($IC_{50} = 2.5$ μmol/L), suggesting that PAK kinases play an extremely important role in their proliferation/survival.

To explore the role of individual PAK isoforms in the observed PF activity, we examined changes in total PAK1/2 proteins as well as phospho PAK1/2/4 following 1 hour of PF treatment at 2.0 to 2.5 μmol/L, which are below the majority of 48 hours IC_{50} values for the selected samples including six J-ATLL cell lines and four NA-ATLL samples (Fig. 2D). Both PAK1 and PAK2 were readily detected in all samples examined except ED40515(+), which has the lowest levels of both PAKs. Lower levels of total PAK1 was also

Published OnlineFirst March 12, 2019; DOI: 10.1158/1078-0432.CCR-18-3033

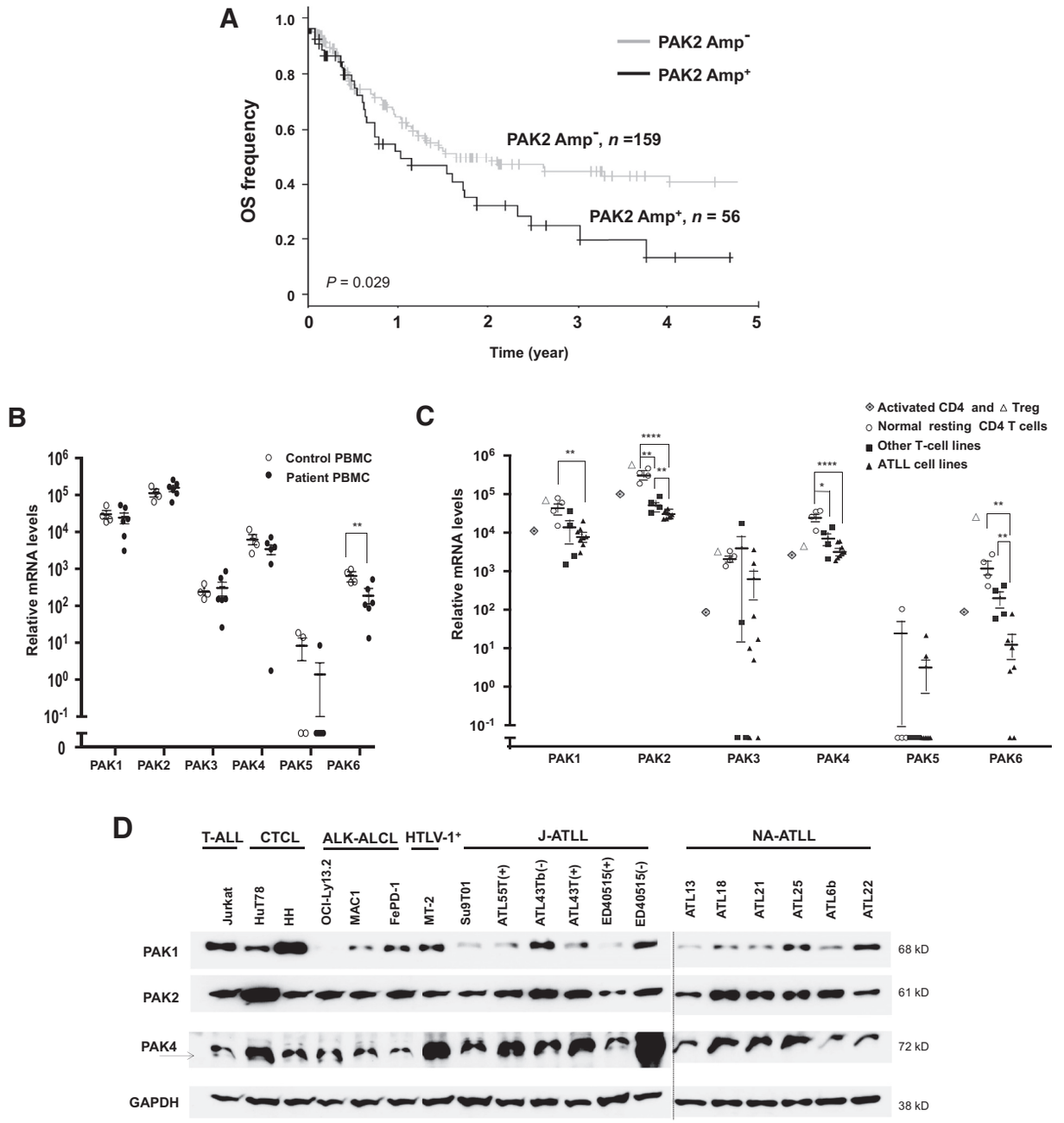

Figure 1.

PAK2 is the most abundantly expressed PAK family member in ATLL, and its amplification is associated with inferior outcome. **A,** OS of patients with ATLL with *PAK2* gene amplification is worse than those without the amplification. **B** and **C,** Quantitative RT-PCR analysis of mRNA levels of PAK family members (**B**) in ATLL patient PBMCs ($n = 6$) compared with healthy control PBMCs ($n = 4$), and (**C**) in ATLL cell lines ($n = 6$) compared with resting ($n = 4$) and activated normal CD4 T cells, normal Treg cells, and cell lines representing other T-cell malignancies ($n = 4$). Error bar, mean ± SEM. Two tailed Student *t* test: *, $P \leq 0.05$; **, $P \leq 0.01$; ****, $P \leq 0.0001$. **D,** Western blot analysis of PAK1, PAK2, and PAK4 protein expression in a panel of T-cell lines and three short-term ATLL cultures (ATL6b, ATL22, and ATL25). Of note, based on data in Supplementary Fig. S2E, the major band reacted with the PAK4 antibody is a nonspecific band, whereas the PAK4-specific signal is the weak band denoted by the arrow.

noted for ATL55T(+) and Su9T01. We examined all four types of phosphorylated PAK1/PAK2 and found that all of them exhibited cell line to cell line variability; yet, there is a close correlation between phospho-Ser20-PAK2 and the ability of a cell line to form tight aggregates in suspension culture (not shown). Interestingly, PF treatment reduced PAK2 phosphorylation on two residues (phospho-Ser20 and phospho-Ser141) while enhancing the signal on the third (phospho-Thr402; Fig. 2D). Because binding of

Published OnlineFirst March 12, 2019; DOI: 10.1158/1078-0432.CCR-18-3033

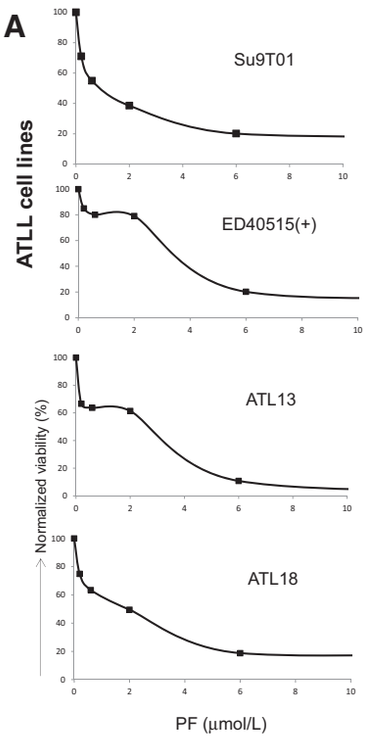

C

Samples			PF-3758309 (μmol/L)	IPA-3 (μmol/L)
Japanese ATLL	Cell lines	ATL43Tb(-)	4.8	15.4
		ATL43T(+)	4.9	16.9
		ATL55(+)	9.3	14.9
		ED40515(-)	7.4	14.0
		ED40515(+)	3.2	10.3
		ED41214(-)	13.4	15.1
		Su9T01	1.8	
North American ATLL	Cell lines	ATL13	5.8	12.0
		ATL18	7.6	
		ATL21	8.0	
	Patient PBMCs	ATL6a	6.4	
		ATL6b	3.2	6.6
		ATL6c	3.8	
		ATL13	14.4	
		ATL18	5.6	
		ATL19a	1.2	
		ATL19b	3.4	
Normal ctrl PBMC			7.2	
Normal activated CD4 T cells			2.5	

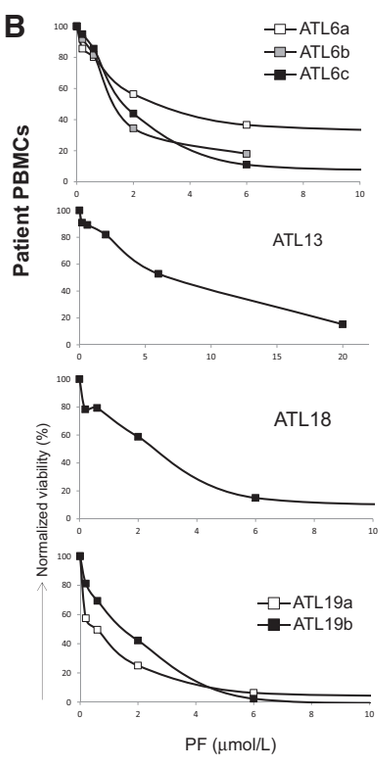

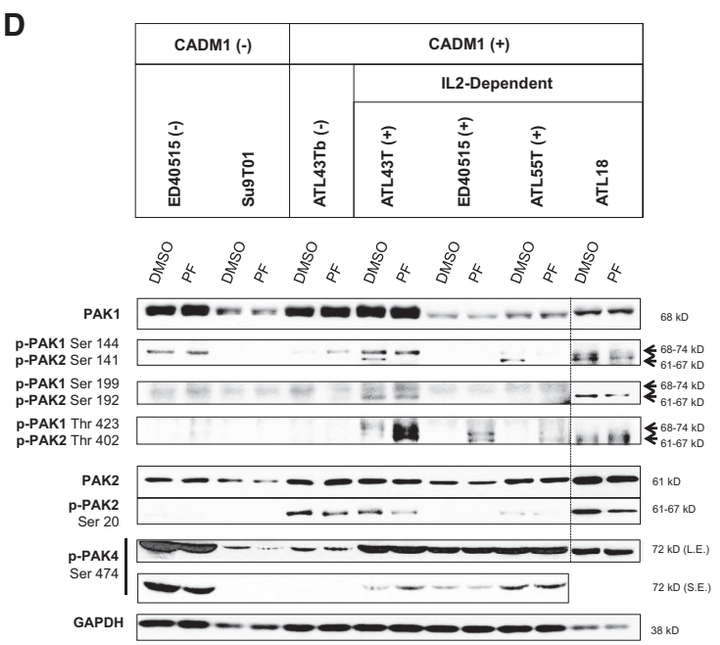

Figure 2.

In vitro response to PAK inhibitors in Japanese and North America ATLL cells. Representative PF response curves of established ATLL cell lines (**A**) and primary patient samples (**B**). Additional PF and IPA-3 response curves are shown in Supplementary Fig. S2. All cultures were treated for 48 hours prior to cell viability measurement with the resazurin assay. **C,** Summary of IC_{50} doses for PF and IPA-3 in all tested samples. PF IC_{50} doses for normal pooled PBMC and activated CD4 T cells are also listed. **D,** Western blot analysis of total and phosphorylated PAK1/2 as well as phosphorylated PAK4 protein in response to 1-hour treatment with PF. All J-ATLL cell lines were treated at 2.5 μmol/L, while the NA-ATLL cell line ATL18 was treated at 2.0 μmol/L. Vertical line has been inserted to indicate a repositioned gel lane.

Published OnlineFirst March 12, 2019; DOI: 10.1158/1078-0432.CCR-18-3033

PF to the primed ATP-binding site in PAK is expected to lock the enzyme in this partially activated state, the observed changes in PAK2 is consistent with the model for its activation (9). In comparison, under the PF treatment conditions, phosphorylated PAK1 was either not altered (phospho-Ser144-PAK1) or often enhanced (phospho-Ser199- and phospho-Thr423-PAK1) but never reduced. In most samples tested, strong phospho-PAK4 signals were detected. Yet, PF only reduced phospho-PAK4 in two cell line, ED40515(−) and Su9T01, which are the most sensitive samples to PF (Fig. 2C). Two conclusions can be made from these observations. First, at 2.0 to 2.5 μmol/L, PF could effectively inhibit PAK2 kinase activity in all samples containing activated PAK2; whereas all seven tested samples contained activated PAK4, it was only reduced by PF in the two sensitive cell lines. Signals representing activated PAK1 were very weak and not reduced in these experiments. Second, when it comes to correlation with in vitro PF response, the best predictor of sensitivity appears to be low level expression of both PAK1 and PAK2 as well as phospho-PAK4 (Fig. 2D).

Pharmacologic PAK inhibition induced time- and dose-dependent apoptosis in ATLL cell lines

Because the resazurin-based *in vitro* viability test measures both cell proliferation and survival effects, we next evaluated these two cellular responses separately. Six J-ATLL and three NA-ATLL cell lines were treated with the indicated doses of PF and apoptosis was measured using Annexin V/PI staining (Fig. 3A; Supplementary Fig. S4). In all samples tested, more apoptotic cells were detected at 48 hours compared with 24 hours, and 10 μmol/L of PF triggered more pronounced apoptotic cell death than 2.0 μmol/L at 24 hours (ATL13 and ATL21; Supplementary Fig. S4). The two most sensitive Japanese cell lines [ED40515(+) and Su9T01] also exhibited the largest apoptotic fractions (40%–50%). Next, we examined cell cycle changes in PF-treated samples (Fig. 3B; Supplementary Figs. S5 and S6). The most significant phenotype was a prominent G_1–S transition block detected in all samples, which was accompanied by corresponding S phase reductions. Variable extent of G_2–M arrest was also observed. In three cell lines showing notable G_2–M accumulation [ATL55T(+), ED40515(+), and ATL43Tb(−) at 40 hours only], CYCLIN B1 and phospho-Ser10 H3 signals were increased thus confirming the activation of G_2 checkpoint. However, this is not the case in ED40515(−) or Su9T01 (Supplementary Fig. S5B).

To determine the molecular mechanisms of PF response, we analyzed three cell signaling molecules (STAT5 and ERK1/2) known to be regulated by PAKs and important for ATLL biology (9, 29, 30). In addition, c-MYC and three apoptosis regulators (MCL1, BAD, and BAX) were also examined. Of note, c-MYC and BAD have previously been shown to be the kinase substrates of PAK2 and PAK1/2, respectively (10). ATLL cells were treated with DMSO or PF for 2, 4, and 8 hours, and whole cell lysates were analyzed by Western blotting (Fig. 3C). The IL-2-independent cell line, ATL43Tb(−), did not contain activated/phosphorylated STAT5. In all three IL-2-dependent cell lines, PAK inhibition notably reduced PY-STAT5 as early as 2 hours into the treatment. Oncogenic c-Myc levels were reduced after PAK inhibition in all samples. Anti-apoptotic MCL1 was also markedly reduced whereas the level of pro-apoptotic BAX was elevated at early stage of the treatment. Because PAK1 can promote ERK1/2 activation independent of its kinase activity (31), we also examined phospho-ERK1/2. All three J-ATLL cell lines showed no or very little phospho-ERK1/2 signals at the baseline, but the two IL-2-dependent lines [ATL55T(+) and ATL43T(+)] upregulated this signal following PF treatment. The cell line ATL18 contained strong phospho-ERK1/2 at the baseline, which was markedly inhibited by PF at 4 and 8 hours, implying that ERK1/2 activation is controlled by different mechanisms in this sample. In the three Japanese cell lines, neither total nor phospho-Ser112-BAD was altered by PF treatment; yet, both were consistently reduced by PF in ATL18 starting from the 2-hour time point. Most of these early changes could still be detectable at 48 hours (Supplementary Fig. S7). The unexpected increase in phospho-BAD may reflect other kinases that can also act on the Ser112 residue (10). Overall, despite the variability in ERK1/2 and BAD, the observed molecular changes were consistent with and likely contributed to the apoptosis and cell-cycle inhibition phenotypes shown in Fig. 3A and B.

Pharmacologic PAK inhibition impaired CADM1-mediated stromal adhesion by ATLL cells

In monotypic suspension culture, primary ATLL cells often form large aggregates, which will dissociate when plated on a feeder layer of HK cells (a human follicular dendritic cell line; ref. 23), mimicking *in vivo* microenvironment (Fig. 4A). Adherence to HK also markedly improved cell viability with unfractionated patient PBMCs and freshly sorted $CD4^+$ leukemic cells (Fig. 4B), suggesting that adhesion-induced cell signaling events regulate both cytoskeletal remodeling and cell death control programs. Because PAKs regulate cancer cell migration and lamellipodia formation by modulating RacGTP activity, and the CADM1–Tiam1–Rac complex has been shown to promote dissemination of ATLL cells *in vivo* (11, 15), we examined the impact of pharmacologic PAK inhibition on the ability of ATLL cells to adhere to HK (Fig. 4C). Using a Calcein AM-based cell adherence assay, we monitored HK adherence of seven ATLL cell lines over a period of 3 hours, comparing the results obtained with and without PF pretreatment. Among the seven cell lines tested, two were CADM1-negative [Supplementary Fig. S8A, Su9T01, ED40515(−)] and neither showed significant HK adherence in 3 hours (Fig. 4C). All five CADM1-expressing cell lines including the ATL18, demonstrated time-dependent HK adherence with variable kinetics. Most importantly, PF pretreatment significantly reduced HK adherence in all five CADM1-expressing cell lines but did not alter the low, basal HK binding activity of the CADM1-negative line, Su9T01. Flow cytometry analysis revealed that defective binding to HK was not due to PF-induced CADM1 downregulation (Supplementary Fig. S8B). These observations support the notion that PAKs positively regulate stromal adherence by CADM1-expressing ATLL cells (Supplementary Fig. S8C).

PAK2 but not PAK1 plays an important role in ATLL stromal interaction

To examine involvement of PAK isoform(s) in the HK adherence process, we analyzed PAK1 and PAK2 protein during the first 150 minutes of ATLL-HK contact in three adhesion-competent cell lines (Fig. 4D). Activated/phospho-Ser144-PAK1 was only detected in ATL43T(+) cells, and was modestly reduced by PF pretreatment. Phospho-Ser141-PAK2 was detected in both ATL43T(+) and ATL55T(+) cells and this signal was nearly

Published OnlineFirst March 12, 2019; DOI: 10.1158/1078-0432.CCR-18-3033

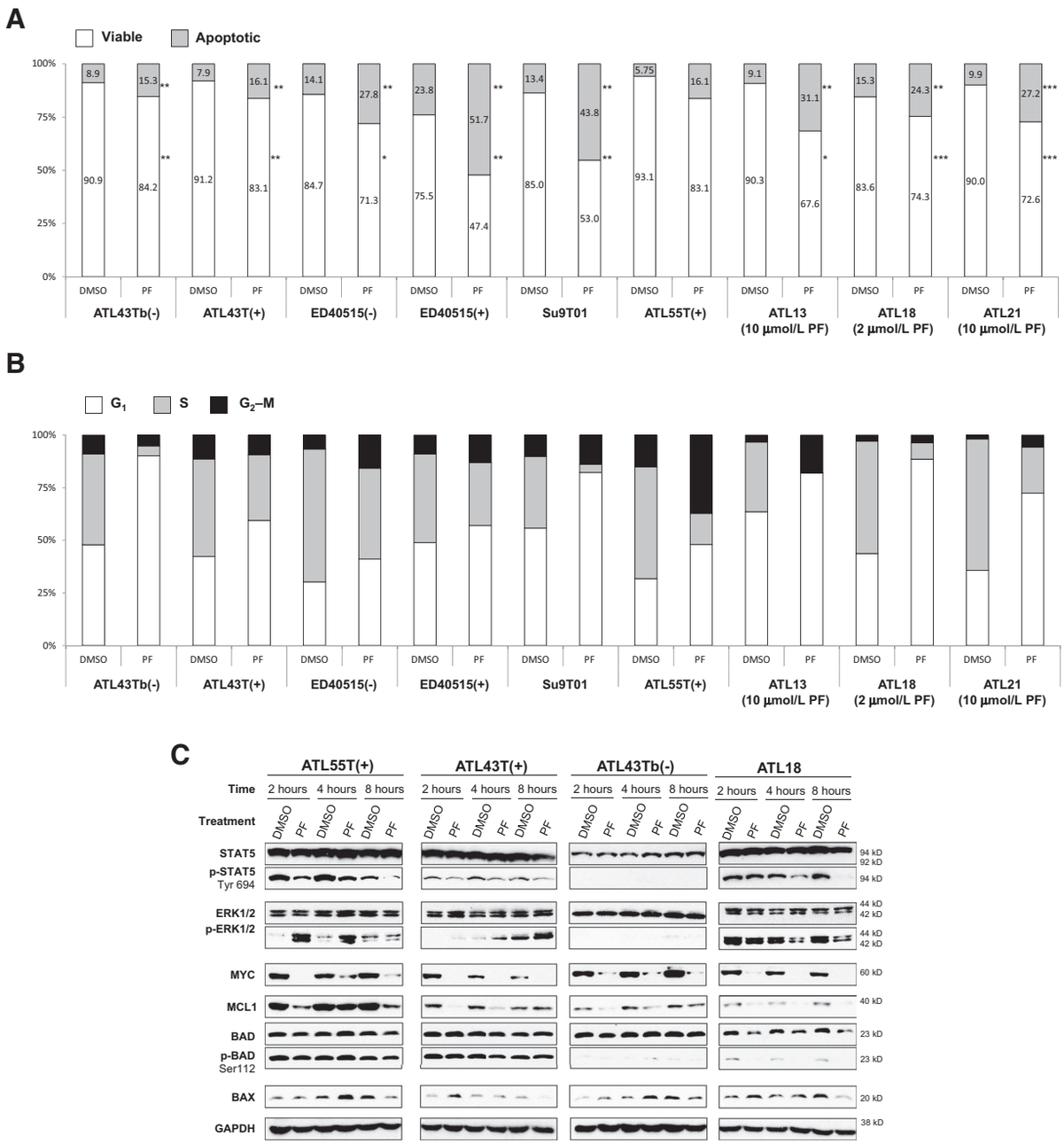

Figure 3.

PAK inhibition induces time- and dose-dependent cytotoxicity in ATLL cell lines. ATLL cell lines exposed to PF for 24 or 48 hours at the indicated concentrations were analyzed by Annexin V (AV)/propidium iodide (PI) staining for apoptosis (**A**) and EdU/PI for cell-cycle changes (**B**). **A,** Viable fraction was defined as AV-negative/PI-negative cells; apoptotic fraction was defined as all AV-positive cells. Results shown are mean two independent experiments. Two-tailed Student *t* test was used for pair-wise comparison as indicated. *, $P < 0.05$; **, $P < 0.01$; ***, $P < 0.001$. Original flow cytometry plots are in Supplementary Fig. S4. **B,** Stacked bar graphs indicate percentage of cells in G_1, S, and G_2–M phases. Original flow cytometry plots for all time points are in Supplementary Figs. S5 and S6. **C,** Western blot analysis of selected proliferation and survival regulators in response to PF treatment for the indicated amount of time. All J-ATLL samples were treated with PF at 2.5 μmol/L, while the doses for the NA-ATLL cell lines are marked in the graph. DMSO, vehicle control.

completely inhibited by PF pretreatment. All cell lines expressed phospho-Ser20-PAK2. This signal as well as total PAK2 were reduced after at 30 and 150 minutes following HK exposure in ATL55T(+) and ED40515(+) cells. In ATL43T(+), however, these PAK2 signals appear to be slightly increased after 30 minutes of HK interaction. In all three cell lines, PF pretreatment decreased phospho-Ser20-PAK2 at the baseline (0 minute) and late stage of HK exposure (150 minutes). In summary, changes in total and/or phospho-Ser20-PAK2 but not any of the PAK1 signals correlated with PF-induced adhesion defect.

Published OnlineFirst March 12, 2019; DOI: 10.1158/1078-0432.CCR-18-3033

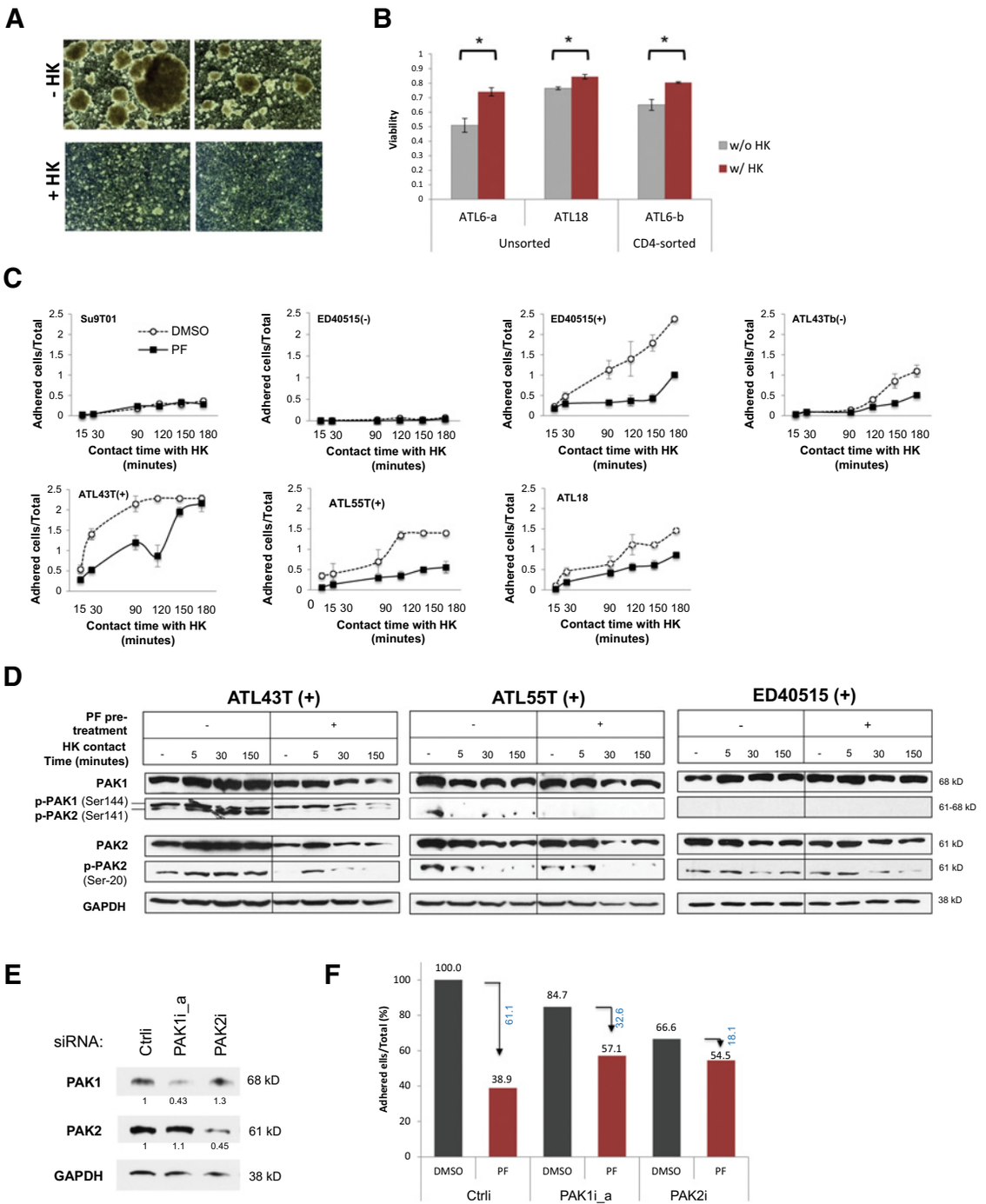

Figure 4.

PAK inhibition impaired stromal adhesion by CADM1-positive ATLL cells. **A,** Interaction with a lymph node stromal cell line, HK, disrupted homophilic cell-cell interaction among primary ATLL cells. **B,** Exposure to HK feeder for 2 days significantly enhanced viability of primary ATLL cells. Viability was assessed based on the Trypan Blue exclusion method. Results shown are mean ± SD. *, $P < 0.01$. **C,** Binding of ATLL cells to the HK feeder was measured in a 3-hour time course using the Calcein AM-based adherence assay. To measure the impact of PAK inhibition, ATLL cells were pretreated with PF at 2.5 μmol/L for 1 hour prior to exposure to the HK feeder. Results shown are representative of at least two independent experiments. **D,** Impact of PF pretreatment on PAK1 and PAK2 activation following adherence to the HK feeder. Before exposure to the HK feeder, ATLL cells were pretreated with PF at 2.5 μmol/L for 1 hour. Whole cell extracts were prepared at the indicated time points and analyzed by Western blotting for the indicated markers. **E,** Effect of siRNA-mediated PAK1 and PAK2 knockdown in ATL55T(+) cells was demonstrated by Western blot analysis 48 hours after siRNA transfection. **F,** HK binding capability of PAK1 and PAK2 KD cells in **E** was evaluated as described in **C**. Relative adhesion measured at 3-hour after HK exposure is shown. Percentage reduction by PF is calculated using the adhesion of DMSO-treated PAK1/2 KD cells as 100% (numbers in blue).

Published OnlineFirst March 12, 2019; DOI: 10.1158/1078-0432.CCR-18-3033

To directly evaluate the function of individual PAK isoforms, we turned to siRNA-based knockdown (KD) approach. Both PAK1 and PAK2 were substantially and specifically reduced at 48 hours following siRNA transfection in ATL55T(+) (Fig. 4E). Interestingly, we observed cross-talk between PAK1 and PAK2 because PAK1 protein was increased in PAK2 KD cells. We then subjected these cells to 1 hour pretreatment by PF before analyzing their capability to adhere to the HK feeder. As shown in Fig. 4F, PAK1 KD by itself reduced HK binding capability by 15.3% and 32.6% of the remainder can be further suppressed by PF. In comparison, PAK2 KD lead to 33.3% loss of HK binding capability and the remainder activity was largely resistant to PF (PF-associated binding loss was only 18.1%). Because PAK1 level increased in PAK2 KD cells, the result indicates that the loss of PAK2 function in cell adhesion could not be compensated by PAK1. Combined with the observations in Fig. 4D, these data suggest that PAK2 is the major target of PF activity in the HK adhesion assay whereas PAK1 has a minor contribution. This conclusion is further supported by time course analysis of PAK1 and PAK2 KD cells in adhesion test (Supplementary Fig. S8D).

PAK2 but not PAK1 promotes cell autonomous ATLL cell survival

Using siRNA-mediated KD approach, we also examined the role of PAK1 and PAK2 in cell proliferation and survival in ATL55T(+) and ATL43Tb(−) cells. ATL55T(+) cells underwent moderate and substantial apoptosis following PAK1 and PAK2 KD, respectively (Fig. 5B; Supplementary Fig. S9A); yet, PAK1 or PAK2 KD did not alter survival of ATL43Tb(−) cells (Fig. 5B; Supplementary Fig. S9B). We did not observe notable cell cycle changes in either cell lines (Supplementary Fig. S9C). As to the molecular changes that may account for the apoptosis phenotype following PAK1 and PAK2 KD, we observed a reduction in total- and PY-STAT5, p-ERK1/2, and MCL1 proteins 72 hours following siRNA transfection (Fig. 5C). The pro-apoptosis protein BAD was elevated at 48 hours only. Interestingly, similar changes were also

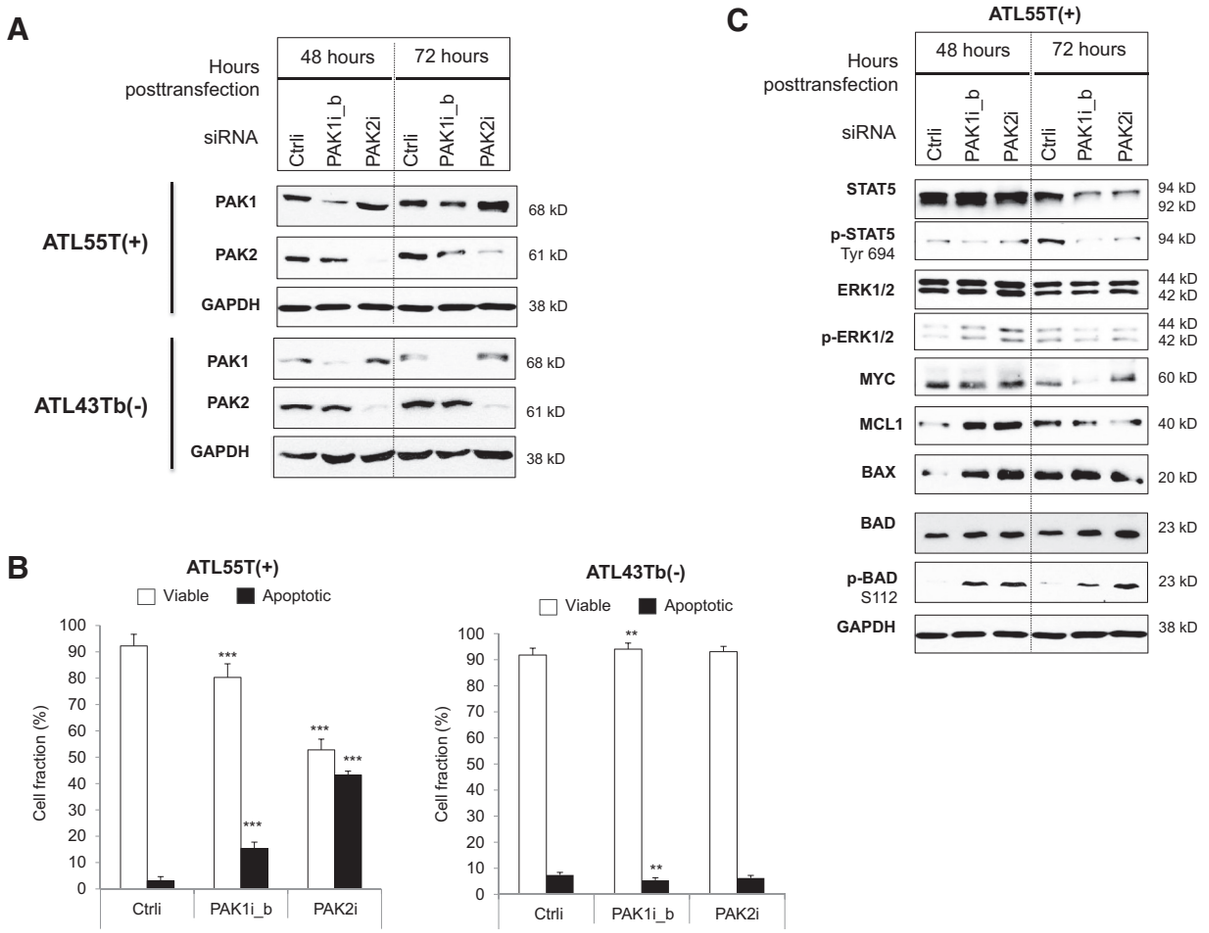

Figure 5.

Roles of PAK1 and PAK2 in ATLL cell proliferation and survival. **A,** Effect of siRNA-mediated PAK1 and PAK2 KD in ATL55T(+) and ATL43Tb(−) cells was demonstrated by Western blot analysis of samples harvested 48 hours after siRNA transfection. **B,** Apoptosis in these two cell lines was measured by AV/PI staining 72 hours after transfection with either PAK1- or PAK2-specific siRNA oligos. Viable fraction was defined as AV-negative/PI-negative cells; apoptotic fraction was defined as all AV-positive cells. Results shown are mean ± SD and representative of two independent experiments. Two-tailed Student *t* test was used for pair-wise comparison as indicated. **, $P < 0.01$; ***, $P < 0.001$. **C,** Impact of siRNA-mediated PAK1 or PAK2 KD on selected cell proliferation and survival regulators in ATL55T(+) was analyzed by Western blotting. Vertical line has been inserted to indicate a repositioned gel lane. Results shown are representative of two independent experiments. Results from ATL43Tb(−) cells are in Supplementary Fig. S10.

Published OnlineFirst March 12, 2019; DOI: 10.1158/1078-0432.CCR-18-3033

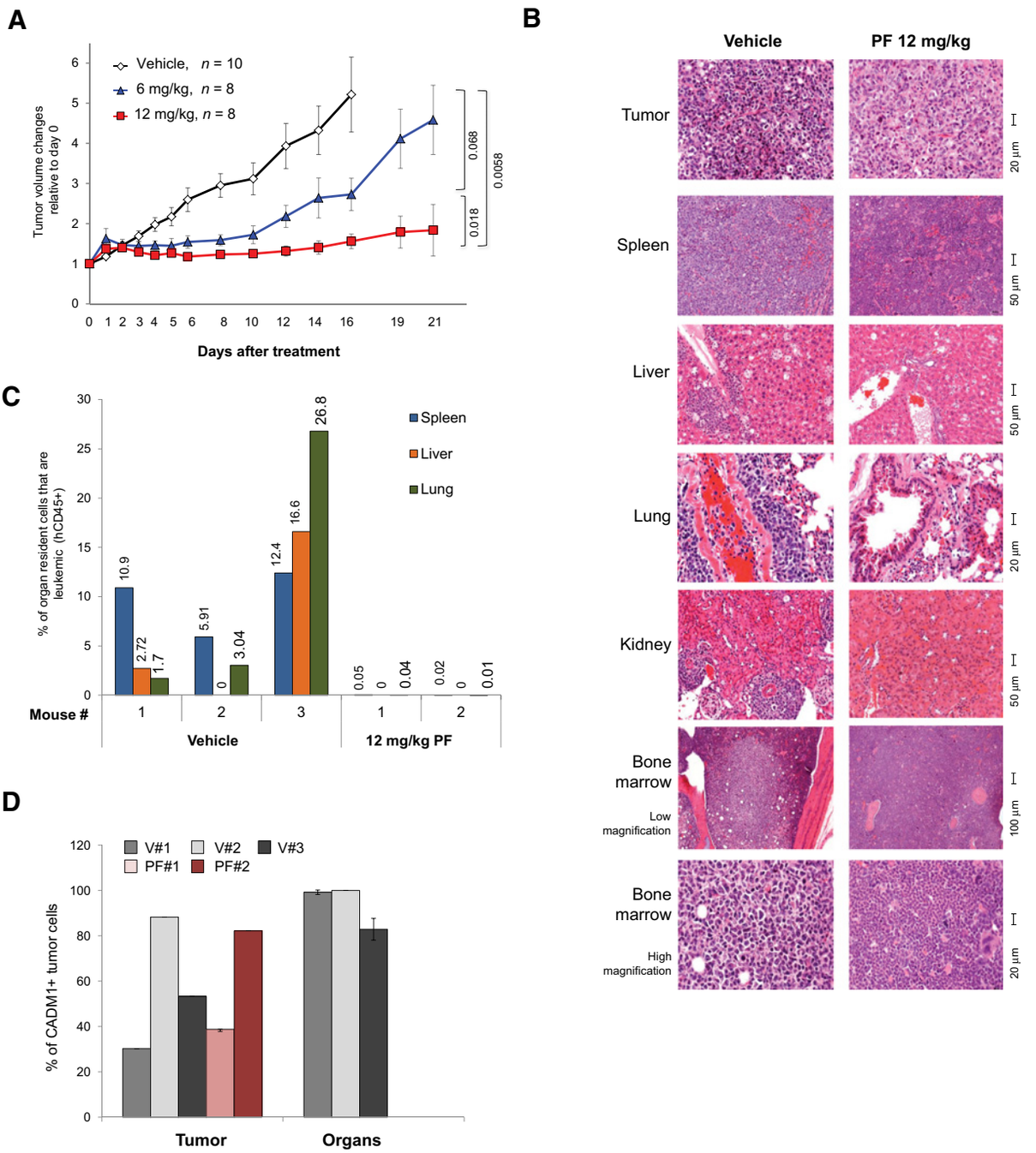

Figure 6.

PF treatment potently inhibited tumor growth and distal dissemination in an ATLL PDX model. **A,** PF has strong and dose-dependent activity in preventing tumor growth at the subcutaneous site. NSG mice bearing ATL18-derived tumor mass were randomly assigned to three treatment arms: vehicle control, 6 or 12 mg/kg i.p. doses daily. Results presented are mean normalized tumor volumes with error bars indicating standard error of the mean. *P* values from group comparisons on day 16 are marked on the right of the graph (two-tailed Student *t* test). **B,** Histologic appearance of subcutaneous tumor mass and major organs from vehicle and 12 mg/kg PF treated mice. Animals were euthanized on day 19 posttreatment. **C,** Enumeration of ATLL cells disseminated to spleen, liver, and lung in the vehicle and 12 mg/kg PF treatment groups. Animals were euthanized after 29 or 36 days of treatment. The number of leukemic cells was quantified using hCD45 staining followed by flow cytometry. **D,** Expression of CADM1 is nearly ubiquitous in disseminated ATLL cells but highly variable in the subcutaneous tumor mass. Results shown are percentage of CADM1-positive cells within the hCD45+ gate. V#1, V#2, and V#3, 3 animals from the vehicle group. PF#1 and PF#2, two mice from the 12 mg/kg PF treatment group. Tumor, subcutaneous tumor mass; organs, averaged percentage of CADM1+ cells in spleen, liver, and lung.

Published OnlineFirst March 12, 2019; DOI: 10.1158/1078-0432.CCR-18-3033

detected in the apoptosis-resistant ATL43Tb(−) cell line except PY-STAT5, which is absent at baseline in this IL-2-independent cell line (Supplementary Fig. S10). This raises an interesting question as to whether PY-STAT5 is a critical mediator of PAK1/2 function in cell survival.

PAK inhibition has potent activity in xenograft-based ATLL animal models

In addition to the NA-ATLL cell lines, we have also established and characterized PDX models using primary samples from our patients. In these models, distal tissue/organ dissemination from subcutaneous engraft site is a prominent feature and the pattern is similar to human ATLL (Fig. 6B). Using a PDX models derived from ATL18 and a CDX model derived from ATL43Tb(−), we evaluated *in vivo* anti-ATLL activity of PF. In the initial experiment using the CDX model, PF administered at 12 mg/kg twice a week achieved significant TGI in 19 days (TGI = 54.9%; Supplementary Fig. S11A). We then initiated a follow up study using the PDX model, where PF was administered daily over a period of 3 weeks (Fig. 6A). At the 12 mg/kg daily dose, PF nearly completely inhibited the subcutaneous tumor growth (TGI = 86.8% on day 16), whereas a substantial albeit more moderate inhibitory effect was achieved with 6 mg/kg (TGI = 59.0% on day 16). Ki67 staining revealed reduced cell proliferation in the subcutaneous tumor mass in PF-treated animal; however, TUNEL-based apoptosis assay did not detect notable differences due to PF treatment (Supplementary Fig. S11D). Most importantly, PF completely prevented distal dissemination of leukemic cells from the subcutaneous site. This is evident from the histology of spleen, liver, lung, kidney, and bone marrow (Fig. 6B) as well as human CD45-based flow cytometry quantification of infiltrating leukemic cells (Fig. 6C). We also examined CADM1 expression pattern at different sites of disease presentation. In keeping with a requirement for CADM1 in tissue/organ infiltration by ATLL cells, nearly all leukemic cells located in internal organs expressed this adhesion molecule (83%–100%) whereas in the subcutaneous site, CADM1 expression was much more variable (30.3%–88.3%) (Fig. 6D). These results demonstrate that PF has potent anti-ATLL activity in xenograft ATLL models where it can strongly inhibit not only *in situ* tumor growth but also distal tissue/organ dissemination. Based on the overall health status, body weight change, and heart histology, the PF treatment protocol did not cause measurable, off-site toxicity in the test animals (Supplementary Fig. S11B and S11C).

Discussion

ATLL is a very aggressive T-cell malignancy with no effective therapy (1, 3, 5). Motivated by the observation that PAK2 is amplified in 24% of Japanese patients with ATLL (8), we examined therapeutic activity of PAK inhibition and characterized roles of PAK family kinases in this disease. We report there that PAK1/2/4 are the three most abundantly expressed PAK isoforms in ATLL. Functional studies demonstrate that the pan-PAK inhibitor PF has strong *in vitro* and *in vivo* anti-ATLL activity in a number of preclinical models. The observed activity of PF is likely attributed to its ability to target several PAK isoforms simultaneously because genetic silencing of either PAK1 or PAK2 only produced variable and moderate cytotoxicity. PAK2, but likely not PAK1, is the major mediator of CADM1-mediated stromal interaction, which is an important step in systemic dissemination of the disease. This is consistent with the observation that PAK2 is more frequently amplified in the aggressive subtypes of ATLL.

Among the six PAK isoforms, PAK2 and PAK4 are ubiquitously expressed, whereas the other four are restricted to specific tissue/organs (9, 32). In all ATLL samples tested, *PAK2* mRNA is the most abundantly expressed followed by *PAK1* and *PAK4* (Fig. 1B and C). The protein products of all three of these genes can be readily detected in ATLL samples tested (Fig. 1D). Although PAK1 and PAK2 have virtually identical substrate specificities, they play different and nonredundant roles in development and cancer (32). For example, PAK1 but not PAK2 have been implicated as a direct regulator of nuclear gene expression program by phosphorylating transcription factors CtBP and STAT5 (29, 33, 34). For cytoskeletal remodeling, rapid turnover of focal contacts at the leading edge of migrating breast cancer cells requires PAK1 (35, 36), whereas modulation of RhoA activity during master cell degranulation is controlled by PAK2 but not PAK1 (37, 38). In this study, we have found that ATLLs under-express *PAK2* mRNA relative to normal CD4 T cells and other T-cell malignancies (Fig. 1C; Supplementary Fig. S2D); yet, PAK2 protein levels appear to be comparable to those found in other T-cell malignances (Fig. 1D) implying additional posttranscriptional regulation. We also found that PAK2 has a more important contribution than PAK1 to stromal adhesion and cell survival in ATLL cells (Figs. 4F and 5B). It is therefore possible that as a disease category, ATLLs tend to under-express *PAK2* mRNA, and this may have rendered PAK2 levels limiting for *in vivo* disease progression, and hence PAK2-amplification events are positively selected in aggressive ATLLs.

We selected PAK1 and PAK2 for gene-specific functional studies since they are the most abundantly expressed PAKs in ATLL. Knockdown experiments showed that the contribution of these two genes to cell autonomous proliferation and survival is not universal. In ATL43Tb(−) cells grown in suspension, they play negligible roles; in ATL55T(+), PAK2 KD caused significant apoptosis while PAK1 KD-induced cell death was more modest. Given the fact that the PF IC_{50} dose for ATL55T(+) is nearly twice of that for ATL43Tb(−) (Fig. 2A) and yet ATL55T(+) was more sensitive to PAK1/2 KD, it is possible that targets other than PAK1 and PAK2 also mediated PF toxicity in the *in vitro* drug sensitivity tests. One such possibility is PAK4. Among the six Japanese cell lines studied by western blotting, the two most sensitive ones have very low phospho-Ser474-PAK4 signals [Su9T01 and ATL43Tb(−)] (Fig. 2B). Therefore, when all of our findings are considered as a whole, there is a formal possibility that both PAK2 and PAK4 mediated PF-induced toxicity in the *in vitro* toxicity assays. Non-PAK kinases that could be targeted by PF under our experimental conditions could also be involved (24).

Multi-organ involvement is the cause of mortality in ATLL. Therefore, ATLL treatment must effectively block systemic dissemination of leukemic cells. Two experiments in this study addressed this issue. In the adherence assays, PF significantly inhibited CADM1-dependent interaction with HK largely through PAK2 (Fig. 4). Although the importance of CADM1 in ATLL progression and systemic dissemination has been documented in the literature (11, 13, 14), this is the first time that a specific member of PAK is shown to operate downstream of CADM1 in this disease. Because stromal interaction significantly enhanced survival of primary ATLL cells (Fig. 4A and B), and this process is largely PAK2-dependent, PAK2 is expected to function as a major survival factor in ATLL microenvironment as well. It is worth

Published OnlineFirst March 12, 2019; DOI: 10.1158/1078-0432.CCR-18-3033

noting here that, in our xenograft study, PF dosed daily at 12 mg/kg potently inhibited subcutaneous tumor growth and completely prevented distal dissemination of leukemic cells (Fig. 6). Combined with the results from our biochemical analysis and PAK1/2 knockdown experiments, such PF activities should be largely attributed to PAK2 with minor contributions from other PAK isoforms, such as PAK1 and PAK4.

In summary, our findings in this study showed that PAK2, a gene frequently amplified in ATLL, facilitates CADM1-mediated stromal interaction and promotes ATLL cell survival. Furthermore, PAK inhibition through an inhibitor such as PF may hold great promise as a targeted therapy for aggressive ATLLs. Although PF was withdrawn from further clinical testing due to inadequate oral availability, additional PAK inhibitors have since been designed (24) and some of them may possess a favorable therapeutic window for a disease associated with frequent PAK2 amplification.

Disclosure of Potential Conflicts of Interest

U. Steidl reports receiving other commercial research support from GlaxoSmithKline, Bayer Healthcare, and Aileron Therapeutics; holds ownership interest (including patents) in Stelexis Therapeutics; and is a consultant/advisory board member for Pieris Pharmaceuticals, Aileron Therapeutics, Stelexis Therapeutics, and Bayer Healthcare. M. Janakiram is a consultant/advisory board member for Miragen and Seattle Genetics. No potential conflicts of interest were disclosed by the other authors.

Acknowledgments

We are grateful to Drs. Thomas Waldmann and Michael Petrus (NIH/NCI) and Prof. Naomichi Arima (Kagoshima University, Japan) for the gift of the Japanese ATLL cell lines; Prof. Naomichi Arima for valuable advice on establishing ATLL long-term cultures; and Drs. John Chan (City of Hope) and Giorgio Inghirami (Weill Cornell Medical College) for the gift of HH, MAC1, and FePD1 cell lines. We also thank Dr. Jonathan Chernoff (Fox Chase Cancer Center, Philadelphia) for insightful discussion and Dr. Robert Stanley (Albert Einstein College of Medicine) for assisting with the design of PAK inhibitor sensitivity tests. Flow cytometry analyses were performed at the Albert Einstein College of Medicine Flow Cytometry facility, which is supported by an NCI Cancer Center Support Grant (P30CA013330). FACS sorting was performed at the Einstein Human Stem Cell FACS and Xenotransplantation Facility, which is supported by a grant from the New York State Department of Health (NYSTEM Program) for the shared facility (C029154). This work was supported by research grants from the Leukemia & Lymphoma Society Translational Research Project (No. 6471-15); Dr. Louis Skarlow Memorial Trust (B.H. Ye); and Aids Malignancy Consortium grant UM1CA121947 (M. Janakiram). E.Y. Chung and Y. Mai are supported by the Harry Eagle Scholarship from the Department of Cell Biology, Albert Einstein College of Medicine, and U.A. Shah was supported by the hematology/oncology fellowship program, Montefiore Medical Center and Jacobi Medical Center.

The costs of publication of this article were defrayed in part by the payment of page charges. This article must therefore be hereby marked *advertisement* in accordance with 18 U.S.C. Section 1734 solely to indicate this fact.

Received September 14, 2018; revised January 11, 2019; accepted March 6, 2019; published first March 12, 2019.

References

1. Ramos JC. Choices and challenges in the treatment of adult T-cell leukemia/lymphoma. J Oncol Pract 2017;13:495–7.
2. Watanabe T. Adult T-cell leukemia: molecular basis for clonal expansion and transformation of HTLV-1-infected T cells. Blood 2017;129:1071–81.
3. Mehta-Shah N, Ratner L, Horwitz SM. Adult T-cell leukemia/lymphoma. J Oncol Pract 2017;13:487–92.
4. Phillips AA, Shapira I, Willim RD, Sanmugarajah J, Solomon WB, Horwitz SM, et al. A critical analysis of prognostic factors in North American patients with human T-cell lymphotropic virus type-1-associated adult T-cell leukemia/lymphoma: a multicenter clinicopathologic experience and new prognostic score. Cancer 2010;116:3438–46.
5. Zell M, Assal A, Derman O, Kornblum N, Battini R, Wang Y, et al. Adult T-cell leukemia/lymphoma in the Caribbean cohort is a distinct clinical entity with dismal response to conventional chemotherapy. Oncotarget 2016;7:51981–90.
6. Licata MJ, Janakiram M, Tan S, Fang Y, Shah UA, Verma AK, et al. Diagnostic challenges of adult T-cell leukemia/lymphoma in North America—a clinical, histological, and immunophenotypic correlation with a workflow proposal. Leuk Lymphoma 2018;59:1188–94.
7. Shah UA, Chung EY, Giricz O, Pradhan K, Kataoka K, Gordon-Mitchell S, et al. North American ATLL has a distinct mutational and transcriptional profile and responds to epigenetic therapies. Blood 2018;132:1507–18.
8. Kataoka K, Nagata Y, Kitanaka A, Shiraishi Y, Shimamura T, Yasunaga J, et al. Integrated molecular analysis of adult T cell leukemia/lymphoma. Nat Genet 2015;47:1304–15.
9. Radu M, Semenova G, Kosoff R, Chernoff J. PAK signalling during the development and progression of cancer. Nat Rev Cancer 2014;14:13–25.
10. Ye DZ, Field J. PAK signaling in cancer. Cell Logist 2012;2:105–16.
11. Masuda M, Maruyama T, Ohta T, Ito A, Hayashi T, Tsukasaki K, et al. CADM1 interacts with Tiam1 and promotes invasive phenotype of human T-cell leukemia virus type I-transformed cells and adult T-cell leukemia cells. J Biol Chem 2010;285:15511–22.
12. Sasaki H, Nishikata I, Shiraga T, Akamatsu E, Fukami T, Hidaka T, et al. Overexpression of a cell adhesion molecule, TSLC1, as a possible molecular marker for acute-type adult T-cell leukemia. Blood 2005;105:1204–13.
13. Dewan MZ, Takamatsu N, Hidaka T, Hatakeyama K, Nakahata S, Fujisawa J, et al. Critical role for TSLC1 expression in the growth and organ infiltration of adult T-cell leukemia cells in vivo. J Virol 2008;82:11958–63.
14. Kobayashi S, Nakano K, Watanabe E, Ishigaki T, Ohno N, Yuji K, et al. CADM1 expression and stepwise downregulation of CD7 are closely associated with clonal expansion of HTLV-I-infected cells in adult T-cell leukemia/lymphoma. Clin Cancer Res 2014;20:2851–61.
15. Murakami S, Sakurai-Yageta M, Maruyama T, Murakami Y. Trans-homophilic interaction of CADM1 activates PI3K by forming a complex with MAGuK-family proteins MPP3 and Dlg. PLoS One 2014;9:e82894.
16. Pujari R, Hunte R, Thomas R, van der Weyden L, Rauch D, Ratner L, et al. Human T-cell leukemia virus type 1 (HTLV-1) tax requires CADM1/TSLC1 for inactivation of the NF-kappaB inhibitor A20 and constitutive NF-kappaB signaling. PLoS Pathog 2015;11:e1004721.
17. Babagana M, Johnson S, Slabodkin H, Bshara W, Morrison C, Kandel ES. P21-activated kinase 1 regulates resistance to BRAF inhibition in human cancer cells. Mol Carcinog 2017;56:1515–25.
18. Lu H, Liu S, Zhang G, Bin Wu, Zhu Y, Frederick DT, et al. PAK signalling drives acquired drug resistance to MAPK inhibitors in BRAF-mutant melanomas. Nature 2017;550:133–6.
19. Walsh K, McKinney MS, Love C, Liu Q, Fan A, Patel A, et al. PAK1 mediates resistance to PI3K inhibition in lymphomas. Clin Cancer Res 2013;19:1106–15.
20. Zhang Y, Wester L, He J, Geiger T, Moerkens M, Siddappa R, et al. IGF1R signaling drives antiestrogen resistance through PAK2/PIX activation in luminal breast cancer. Oncogene 2018;37:1869–84.
21. Zhao ZS, Manser E. Do PAKs make good drug targets? F1000 Biol Rep 2010;2:70.
22. Pandolfi A, Stanley RF, Yu Y, Bartholdy B, Pendurti G, Gritsman K, et al. PAK1 is a therapeutic target in acute myeloid leukemia and myelodysplastic syndrome. Blood 2015;126:1118–27.
23. Kim HS, Zhang X, Choi YS. Activation and proliferation of follicular dendritic cell-like cells by activated T lymphocytes. J Immunol 1994;153:2951–61.
24. Rudolph J, Murray LJ, Ndubaku CO, O'Brien T, Blackwood E, Wang W, et al. Chemically diverse group I p21-activated kinase (PAK) inhibitors impart acute cardiovascular toxicity with a narrow therapeutic window. J Med Chem 2016;59:5520–41.

Published OnlineFirst March 12, 2019; DOI: 10.1158/1078-0432.CCR-18-3033

25. Yamagishi M, Nakano K, Miyake A, Yamochi T, Kagami Y, Tsutsumi A, et al. Polycomb-mediated loss of miR-31 activates NIK-dependent NF-kappaB pathway in adult T cell leukemia and other cancers. Cancer Cell 2012;21: 121–35.
26. Murray BW, Guo C, Piraino J, Westwick JK, Zhang C, Lamerdin J, et al. Small-molecule p21-activated kinase inhibitor PF-3758309 is a potent inhibitor of oncogenic signaling and tumor growth. Proc Natl Acad Sci U S A 2010;107:9446–51.
27. Rudolph J, Crawford JJ, Hoeflich KP, Wang W. Inhibitors of p21-activated kinases (PAKs). J Med Chem 2015;58:111–29.
28. Deacon SW, Beeser A, Fukui JA, Rennefahrt UE, Myers C, Chernoff J, et al. An isoform-selective, small-molecule inhibitor targets the autoregulatory mechanism of p21-activated kinase. Chem Biol 2008;15:322–31.
29. Chatterjee A, Ghosh J, Ramdas B, Mali RS, Martin H, Kobayashi M, et al. Regulation of Stat5 by FAK and PAK1 in oncogenic FLT3- and KIT-driven leukemogenesis. Cell Rep 2014;9:1333–48.
30. Zhang M, Mathews Griner LA, Ju W, Duveau DY, Guha R, Petrus MN, et al. Selective targeting of JAK/STAT signaling is potentiated by Bcl-xL blockade in IL-2-dependent adult T-cell leukemia. Proc Natl Acad Sci U S A 2015;112: 12480–5.
31. Wang Z, Fu M, Wang L, Liu J, Li Y, Brakebusch C, et al. p21-activated kinase 1 (PAK1) can promote ERK activation in a kinase-independent manner. J Biol Chem 2013;288:20093–9.
32. Kelly ML, Chernoff J. Mouse models of PAK function. Cell Logist 2012;2: 84–8.
33. Barnes CJ, Vadlamudi RK, Mishra SK, Jacobson RH, Li F, Kumar R. Functional inactivation of a transcriptional corepressor by a signaling kinase. Nat Struct Biol 2003;10:622–8.
34. Berger A, Hoelbl-Kovacic A, Bourgeais J, Hoefling L, Warsch W, Grundschober E, et al. PAK-dependent STAT5 serine phosphorylation is required for BCR-ABL-induced leukemogenesis. Leukemia 2014;28:629–41.
35. Brown MC, West KA, Turner CE. Paxillin-dependent paxillin kinase linker and p21-activated kinase localization to focal adhesions involves a multistep activation pathway. Mol Biol Cell 2002;13:1550–65.
36. Nayal A, Webb DJ, Brown CM, Schaefer EM, Vicente-Manzanares M, Horwitz AR. Paxillin phosphorylation at Ser273 localizes a GIT1-PIX-PAK complex and regulates adhesion and protrusion dynamics. J Cell Biol 2006; 173:587–9.
37. Allen JD, Jaffer ZM, Park SJ, Burgin S, Hofmann C, Sells MA, et al. p21-activated kinase regulates mast cell degranulation via effects on calcium mobilization and cytoskeletal dynamics. Blood 2009;113: 2695–705.
38. Kosoff R, Chow HY, Radu M, Chernoff J. Pak2 kinase restrains mast cell FcepsilonRI receptor signaling through modulation of Rho protein guanine nucleotide exchange factor (GEF) activity. J Biol Chem 2013;288: 974–83.

Published OnlineFirst March 12, 2019; DOI: 10.1158/1078-0432.CCR-18-3033

Clinical Cancer Research

PAK Kinase Inhibition Has Therapeutic Activity in Novel Preclinical Models of Adult T-Cell Leukemia/Lymphoma

Elaine Y. Chung, Yun Mai, Urvi A. Shah, et al.

Clin Cancer Res 2019;25:3589-3601. Published OnlineFirst March 12, 2019.

List of Supplementary Material

Supplementary Methods

Supplementary Tables

Supplementary Figures

Supplementary Materials and Methods

Primary peripheral blood mononuclear cells (PBMCs) from ATLL patients and healthy subjects. Anti-coagulated peripheral blood samples were obtained from patients diagnosed with ATLL after Institutional Review Board approval by the Albert Einstein College of Medicine, in accordance with the Declaration of Helsinki. Patient characteristics, including demographics, laboratory parameters, cytogenetics and treatment course including survival, were collected using retrospective chart review[1]. Four healthy volunteers donated peripheral blood samples anonymously. PBMCs were purified from whole blood using Ficoll-Paque-based density centrifugation. Freshly isolated PBMCs were used for total RNA preparation (ATL6a, ATL6d, ATL13, ATL18, ATL20, and ATL21; Fig 1B) and in vitro drug sensitivity tests (ATL6a, ATL6b, ATL6c, ATL13, ATL18, ATL19, ATL21; Fig 2B-C and Fig S2). Total RNA was also isolated from activated CD4 and Treg cells for RT-qPCR.

CD4 isolation. CD4+ human T cells were isolated from PBMCs using CD4 MicroBeads from (Miltenyi Biotec, Cat# 130-045-101). Purity is >95% according to cell surface staining of CD4 positive cells by flow cytometry. Purified CD4+ human T cells were coated at (1X10^5/well) and activated with anti-CD3 antibody (Clone OKT3, Biolegend) coated on 96-well round bottom plate at 5ug/ml together with incubation with soluble rhIL-2 at 1 ng/ml for 3 days. CD4 T cell activation status is determined by cell division (>75% division) by FACs analysis after activation. Treg (CD4+ CD25+) T cells were isolated using Treg isolation kit form miltenly bioteh accoding to manufacturer's instructions. Purity of Treg are ~ 92.5% after isolation as determined by FACS analysis.

Apoptosis, EdU-PI staining and flow cytometry. Cell cultures were exposed to PF-3758309 or upon siRNA-mediated knock down of PAK1 or PAK2. Apoptosis was evaluated using Annexin V-FITC Apoptosis Detection Kit I (BD Biosciences, cat. no. 556547) according to the manufacturer's instructions. The Click-iT EdU kit from Invitrogen (cat # 10424) was used for EdU labeling. Cells were washed twice and resuspended with cold 1 x PBS (+1% BSA). EdU was added to the cells at the final concentration of 10uM for 90min at 37^{o}C, followed by washing with 1 x PBS (+1% BSA). Cells were then fixed/permeablized and incorporated EdU was detected with azide conjugated to the Alexa Fluor 647 fluorochrome according to the manufacturer's instructions. RNaseA and propidium-iodide (PI) at the final concentration of 1mg/ml and 50ug/ml respectively were added to the cells for 30 minutes at 37^{o}C prior to FACS analysis. For CADM-1 cell surface expression, 0.5 x10^{6} cells were washed twice with 1 x PBS (+2% FBS) followed by incubation with 2ul of FcR blocking reagent (Miltenyi Biotec, cat. no. 130-059-901)/100ul of staining buffer, 1 x PBS (+2% FBS), for 30 minutes on ice before staining with CADM-1 Alexa 647 antibody (MBL, cat no. CM004-A64). Cells were analyzed on the FACSCantoII flow cytometer and the results were analyzed using the FlowJo software.

siRNA Transfection. ATL55T(+) and ATL43Tb(-) were electroporated with either control, PAK1 or PAK2 siRNA using the Amaxa electroporation system kit T and L, respectively, according to the manufacturer's instructions. Control siRNA (5′-AACGTACGCGGAATACTTCGA; D-001210-01-05), 2 siRNAs against PAK1: PAK1i_a (5′-GAAGAAATATACACGGTTT; D-003521-01) PAK1i_b (5′-TGAAATGCTCTCGGCTAT; D-

003521-21), PAK2 (5′-GAAGGAACTGATCATTAA; D-003597-05) and PAK4 (5′-GACUGAAGAACCUGCACAATT). siRNAs were purchased from Dharmacon and used at 100 uM final concentration.

Western blotting and quantitative RT-PCR (qRT-PCR). Western blotting and qRT-PCR were performed using standard techniques as previously described[2]. To prepare whole cell protein lysates, cells were lysed at the ratio of $1x10^6$ cells per 80 ul 1x lammeli sample buffer to obtain. 10 ul of protein lysate with the equivalent of 0.125 $x10^6$ cells were loaded per lane on the SDS-PAGE gel. Primary antibodies used are listed in Supplementary Table S1. Total RNA was extracted using Trizol (Invitrogen), and the results from qRT-PCR were normalized using the geometric mean method with 3 housekeeping genes, HMBS, HPRT, and ACTB[3]. Sequences of the primers are listed in Supplementary Table S2.

Histology. FFPE sections were prepared from tumors and organs from animals in the xenograft study. Following standard Hematoxylin and eosin (H&E), Ki-67 and TUNEL staining, slides were photographed through a light microscope.

Statistical analysis. Unpaired 2-tailed Student t-test was performed to compare numerical variables in two sample groups. The Kaplan-Meier method was used to estimate the survival distributions with the log-rank test performed to compare the survival curves. When comparing the frequency of PAK2 amplification in the aggressive versus indolent ATLL cases, the adjusted p-value (q-value) was obtained following Benjamini-Hochberg correction. The statistical analyses were performed with GraphPad Prism 7 or Stata v12 software. Statistical significance was set at a level of $P<0.05$.

References cited.

1. Shah UA, Chung EY, Giricz O, et al. North American ATLL has a distinct mutational and transcriptional profile and responds to epigenetic therapies. *Blood*. 2018.
2. Mendez LM, Polo JM, Yu JJ, et al. CtBP is an essential corepressor for BCL6 autoregulation. *Mol Cell Biol*. 2008;28(7):2175-2186.
3. Vandesompele J, De Preter K, Pattyn F, et al. Accurate normalization of real-time quantitative RT-PCR data by geometric averaging of multiple internal control genes. *Genome Biol*. 2002;3(7):RESEARCH0034.

Figure S1. Characteristics of the 3 North American ATLL cell lines used in this study.

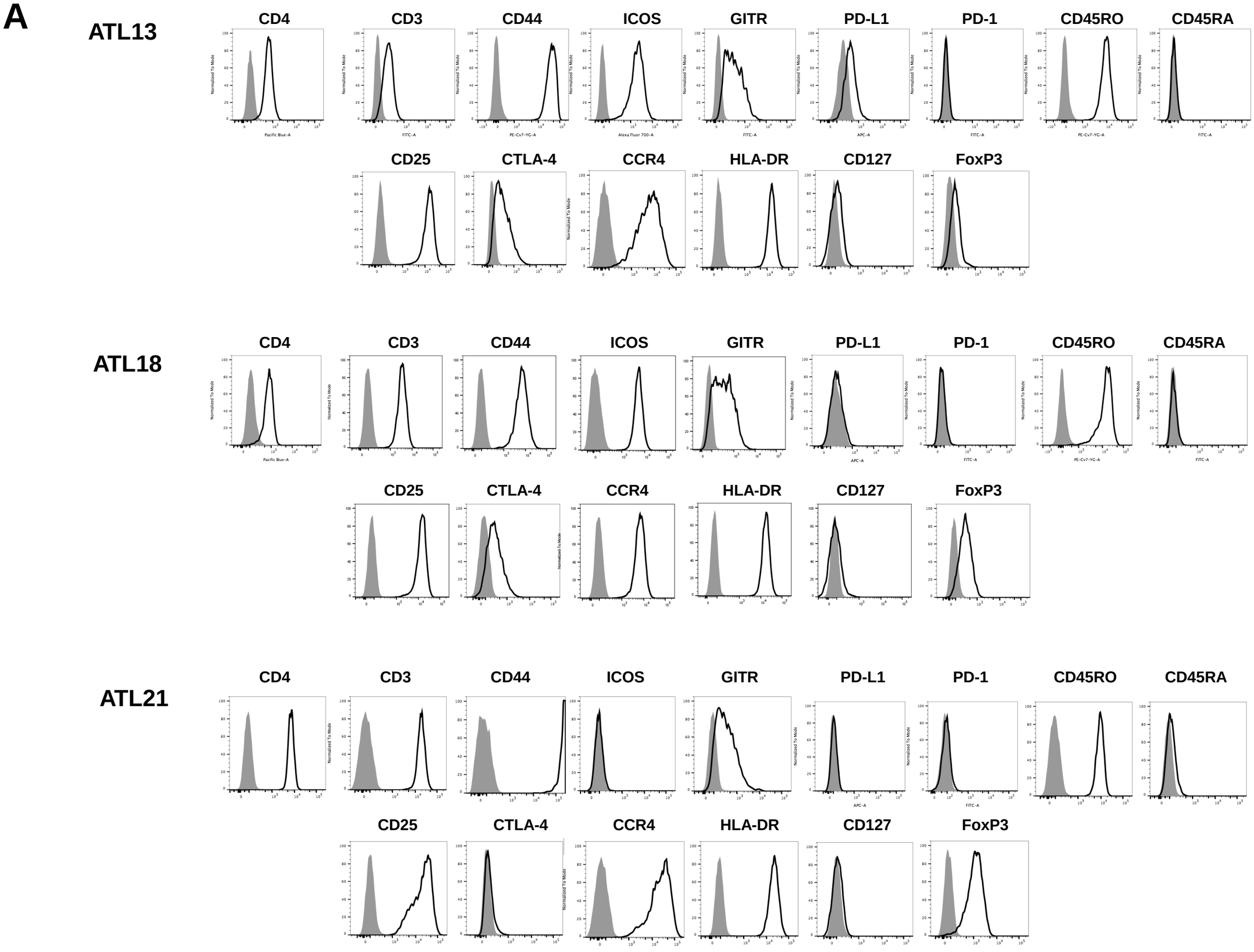

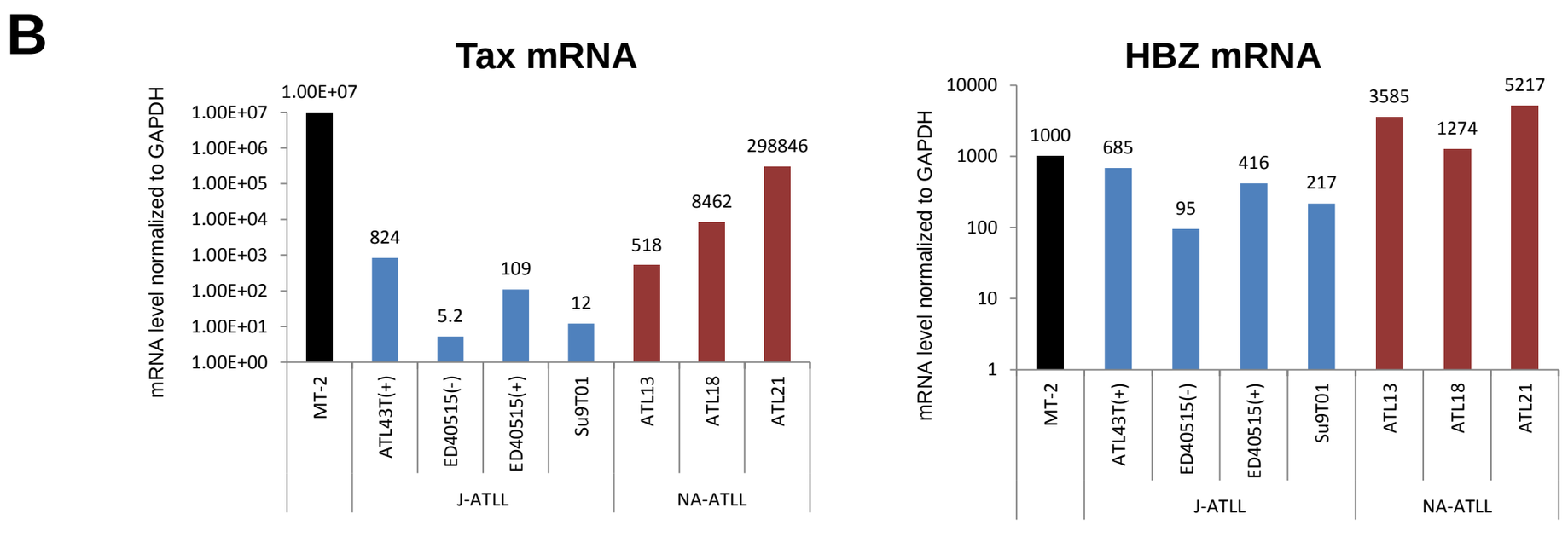

Figure S1. Immunophenotype and viral gene expression status of the three NA-ATLL cell lines.
(**A**) Flow cytometry analysis of 14 T-cell related surface markers as well as the Treg-specific transcription factor FoxP3.
(B) mRNA expression of Tax and HBZ in 4 J-ATLL and 3 NA-ATLL cell lines. The values are normalized to GAPDH. MT-2, a HTLV-1 immortalized human CD4 cell line is included as control.

Figure S2. *PAK2 amplification pattern in ATLL and expression of PAK isoforms in published ATLL datasets.*

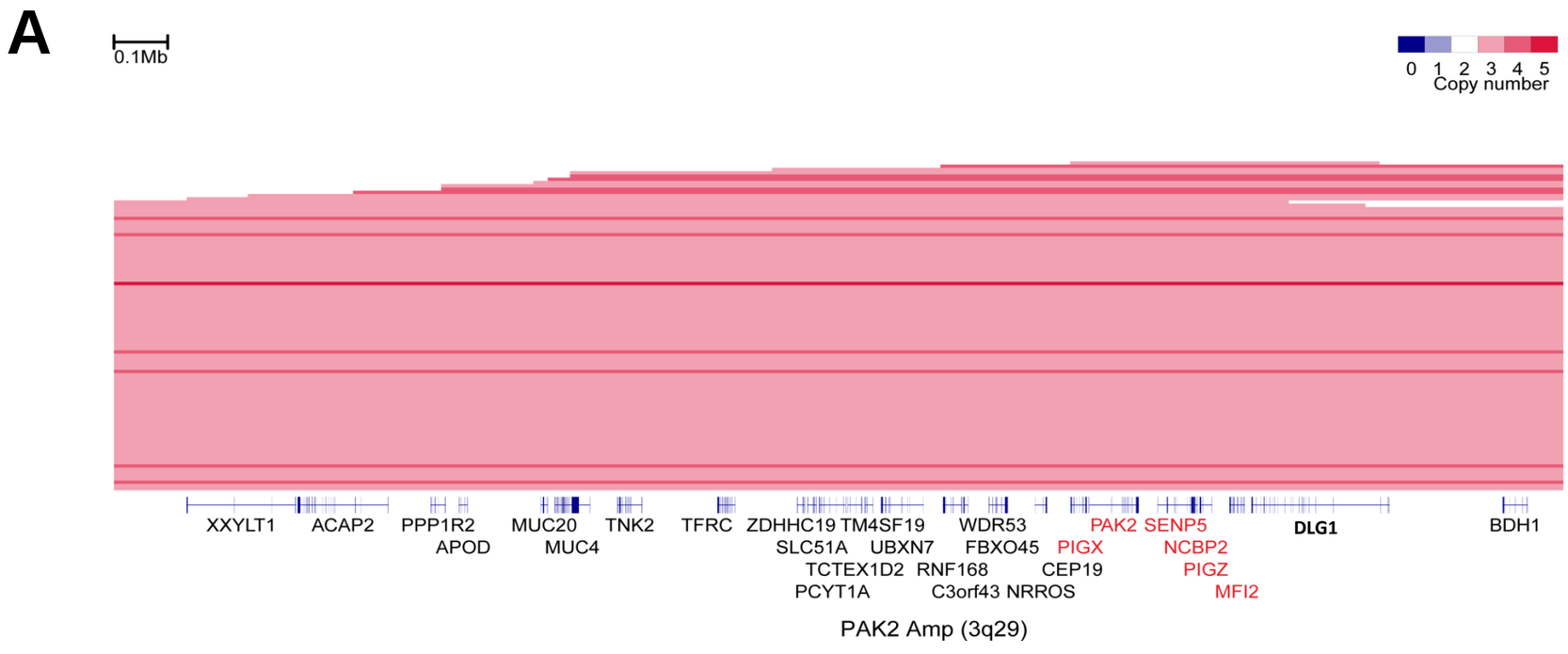

Figure S2 (Results related to Figure 1). PAK2 amplification pattern in ATLL and expression of PAK isoforms in published ATLL datasets.

(**A**) 3q29 focal amplifications involving *PAK2* (n = 101) were detected by GISTIC 2.0 analysis. Segmented copy number data from SNP array karyotyping for 426 ATLL patients are shown. Each row represents a patient, and the genes included in the minimal common region are shown in red.

(B) PAK1 and PAK2 expression levels in PAK2 diploid (n=42) and amplified cases (n=12).

(**C**) Box plot presentation of PAK isoform expression pattern in Japanese ATLL patient samples. RNA-seq data in (B) and (C) are extracted from a previously published RNA-seq dataset (Kataoka K et al, Nat Genet 2015). FPKM (Fragments Per Kilobase of transcript per Million mapped reads). PAK5 data is not shown as this gene is not expressed in ATLLs.

(**D**) Agilent gene chip-based RNA expression patterns for aggressive ATLL, indolent ATLL, and normal CD4 T cell samples are extracted from GSE33615 (Yamagishi M et al, Cancer Cell 2012). The significance levels are based on two tailed Student t test: **, $P<0.01$, ***, $P<0.001$

(**E**) Western Blot analysis of the effects of siRNA mediated knock down experiment reveals that the dominant signal reactive with the Cell Signaling PAK4 antibody (#3242) is non-specific (*). Whole cell lysates of transfected ATL55T(+) cells were harvested 48 hrs after transfection. Specific PAK4 signal is denoted by red arrows.

Chung et al., Figure S2

Figure S3. Survival curves for primary ATLL samples and ATLL cell lines treated with PF or IPA3

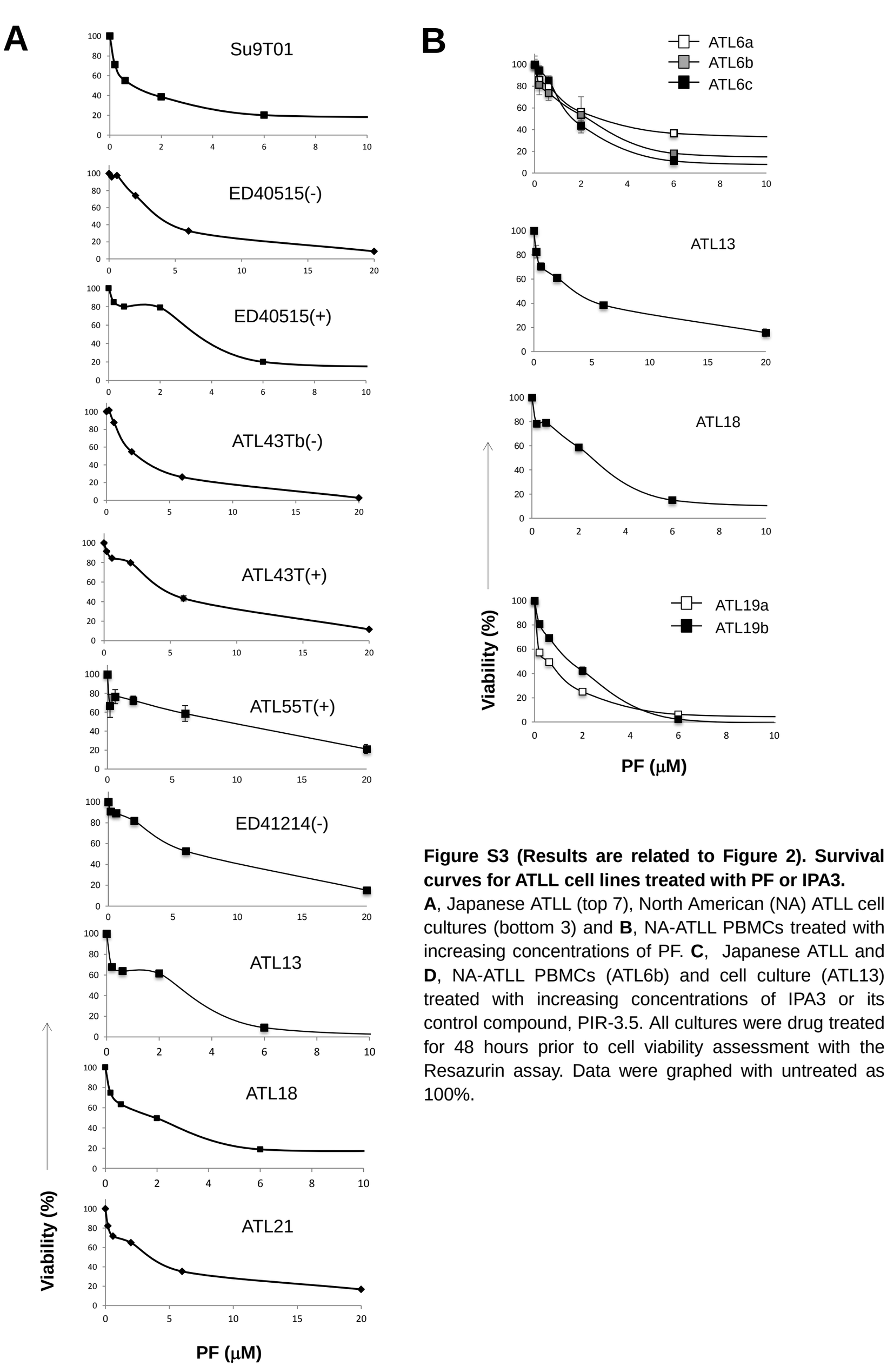

Figure S3 (Results are related to Figure 2). Survival curves for ATLL cell lines treated with PF or IPA3.
A, Japanese ATLL (top 7), North American (NA) ATLL cell cultures (bottom 3) and **B**, NA-ATLL PBMCs treated with increasing concentrations of PF. **C**, Japanese ATLL and **D**, NA-ATLL PBMCs (ATL6b) and cell culture (ATL13) treated with increasing concentrations of IPA3 or its control compound, PIR-3.5. All cultures were drug treated for 48 hours prior to cell viability assessment with the Resazurin assay. Data were graphed with untreated as 100%.

Figure S4. Apoptosis analysis of ATLL cell lines treated with PF for 24 and 48 hours

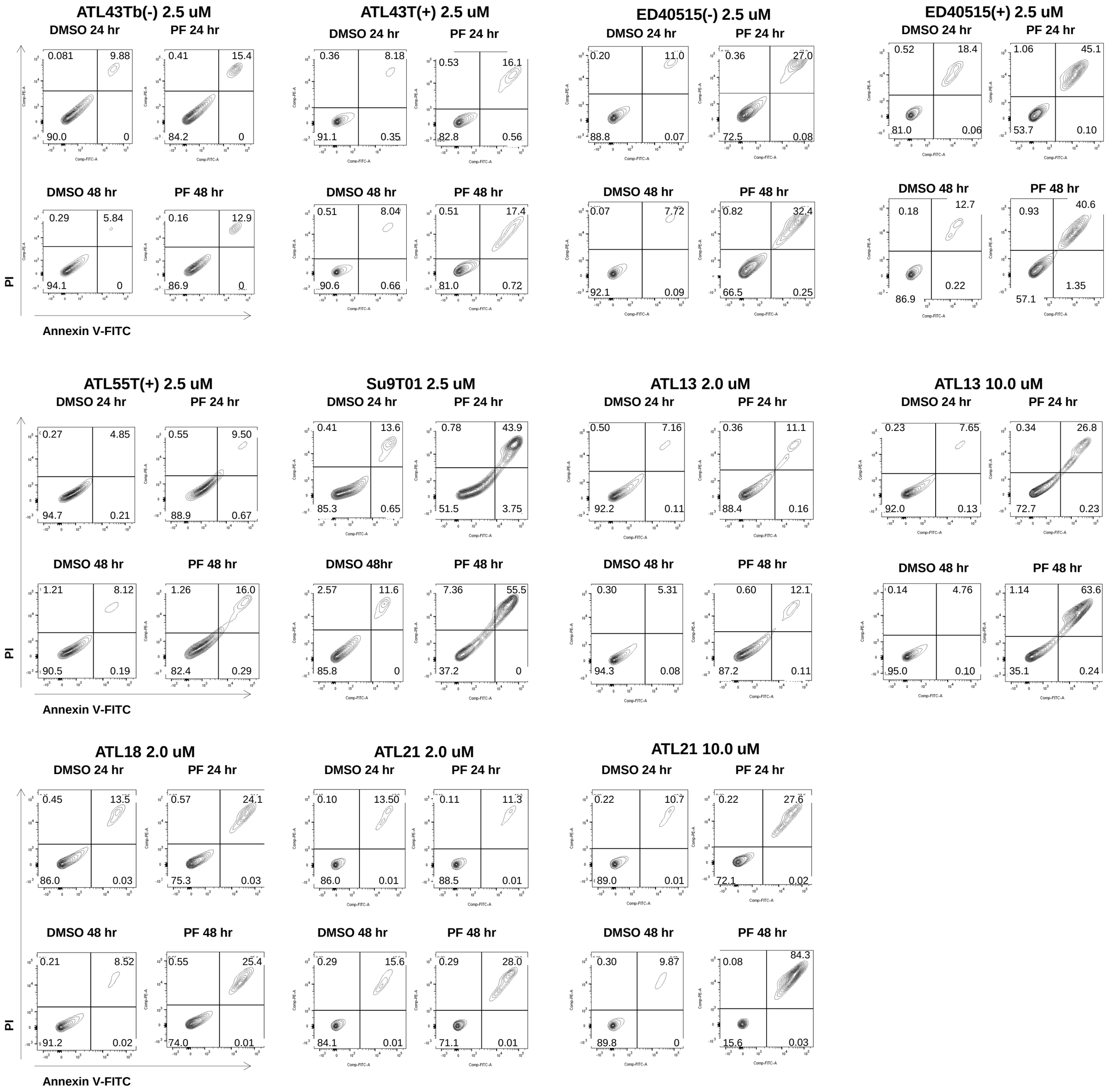

Figure S4 (Results are related to Figure 3A). Annexin V (AV)/Propidium iodide (PI)-based apoptosis analysis of ATLL cell lines treated with PF for 24 and 48 hours. Japanese ATLL (ATL43Tb(-), ATL43T(+), ED40515(-), ED40515(+),ATL55T(+) and Su9T01) and North American ATLL (ATL13, ATL18 and ATL21) cell cultures were treated with PF (dosage as indicated) for 24 and 48 hours followed by apoptosis analysis by AV and PI staining. Representative contour plots with live cells (AV-PI- population) in the bottom left quadrant and apoptotic cells (AV+PI- and AV+PI+ populations) in the lower right and upper left quadrants.

Chung et al., Figure S4

Figure S5. Cell cycle analysis of Japanese ATLL cell lines treated with PF for 24 and 40 hours

A

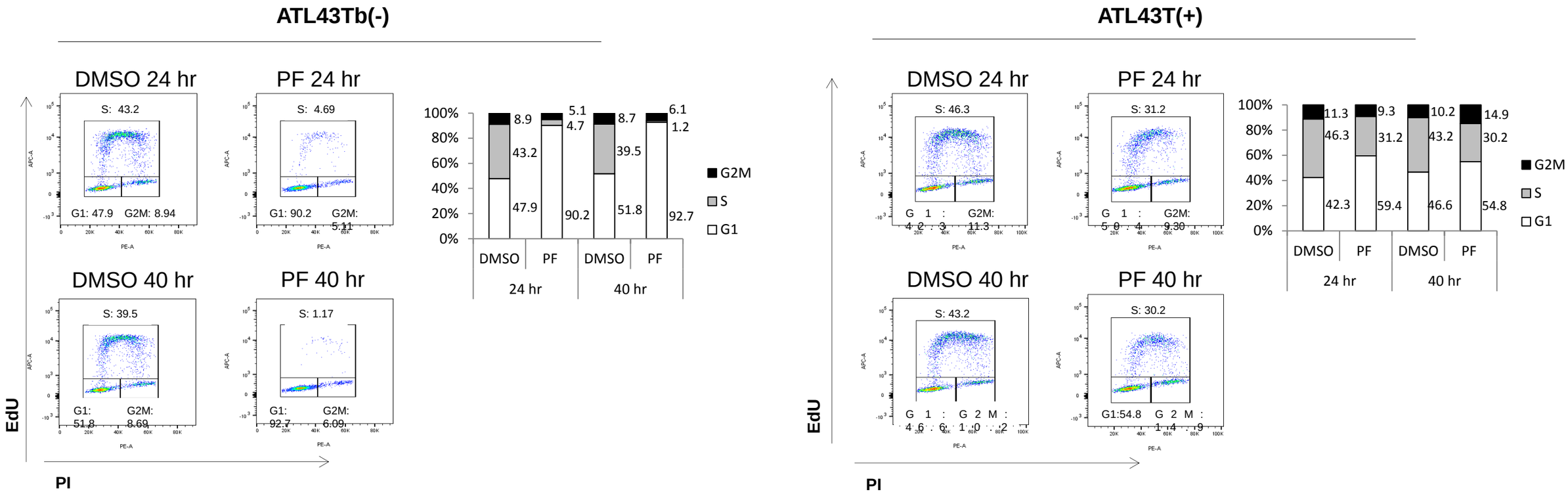

Figure S5 continued on next page.

Figure S5. Cell cycle analysis of Japanese ATLL cell lines treated with PF for 24 and 40 hours

Continued from the previous page.

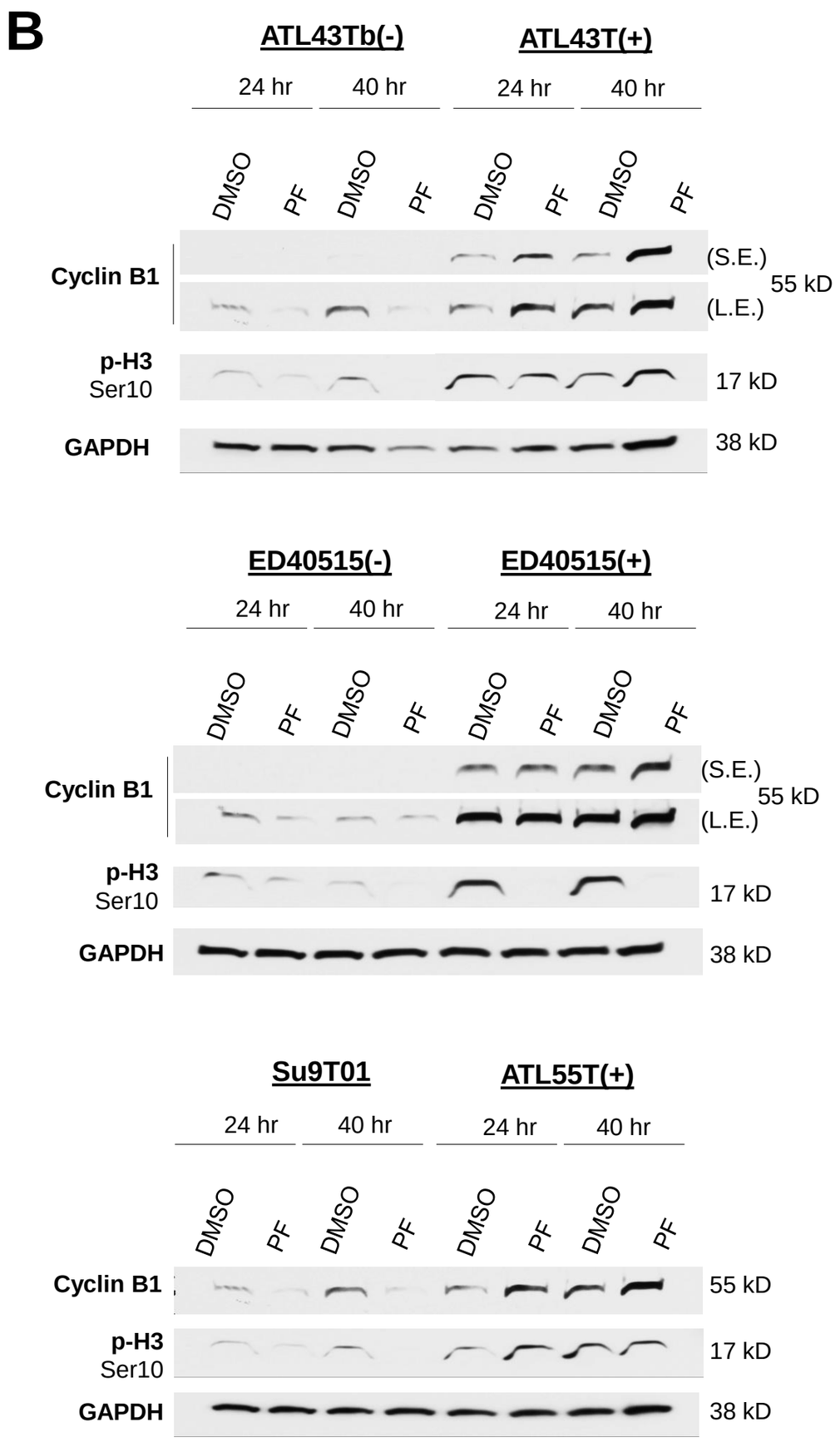

Figure S5 (Results are related to Figure 3B). Cell cycle analysis of 6 Japanese ATLL cell cultures treated with PF for 24 and 40 hours.

(A) Results of cell cycle analysis based on EdU/PI staining. Shown are flow cytometry plots and bar graphs according to the percentage of cells in the G1, S, and G2/M gates.

(B) Whole cell extracts were made from PF-treated cell lines and used for Western blot analysis of Cyclin B1 and phospho-Ser10 H3.

Figure S6. Cell cycle analysis of North American ATLL cell lines treated with PF for 24 and 40 hours

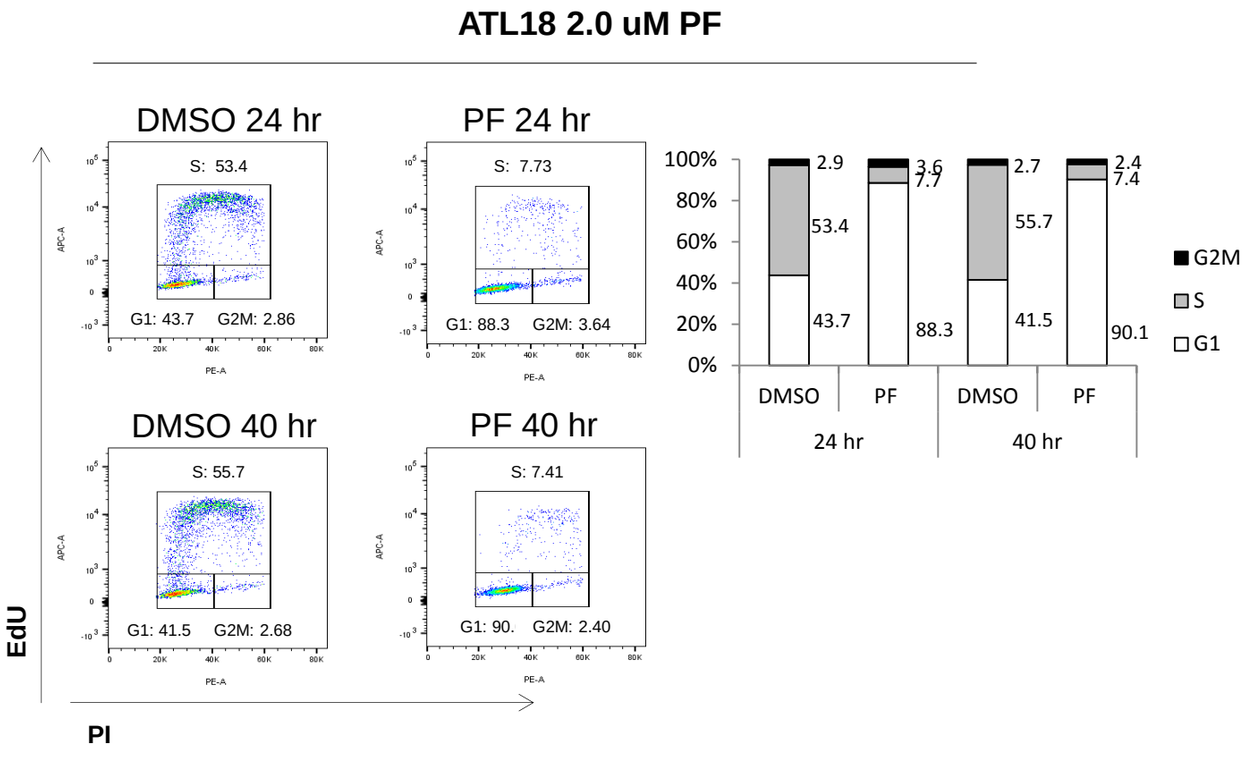

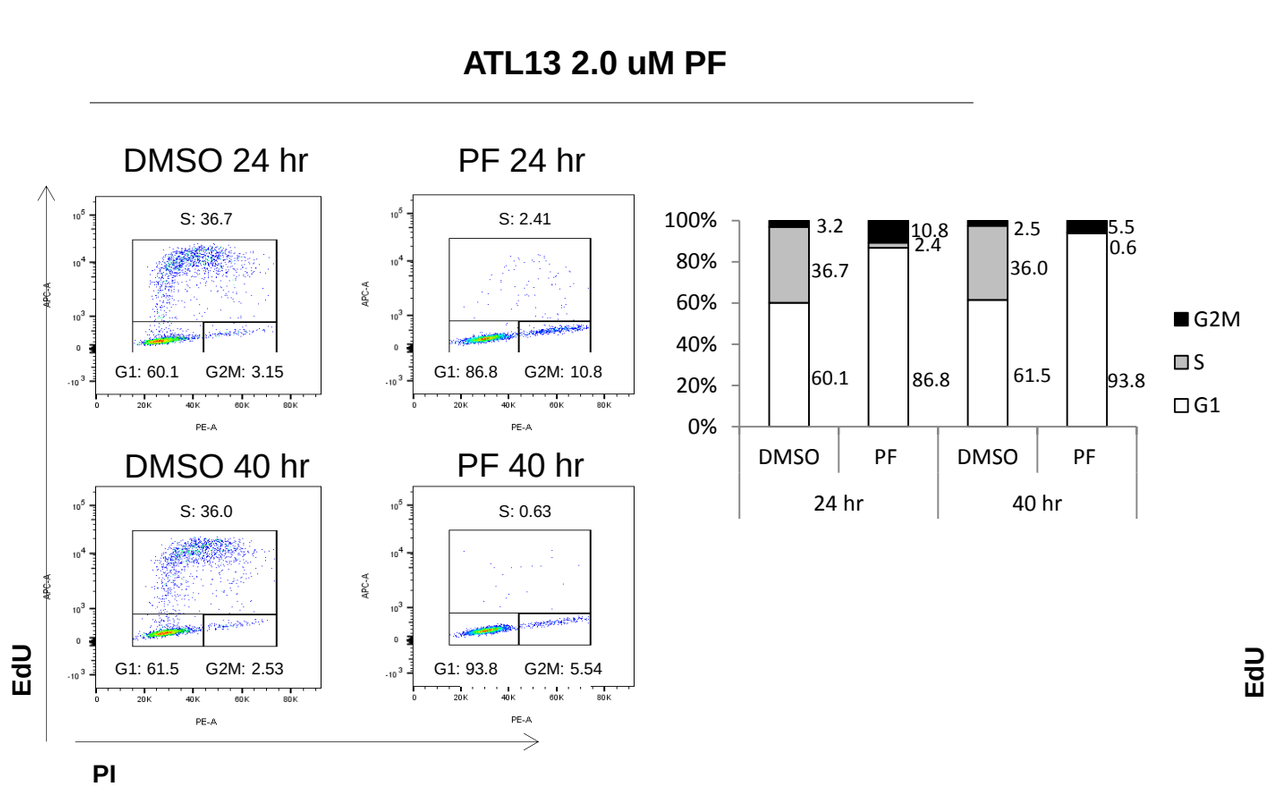

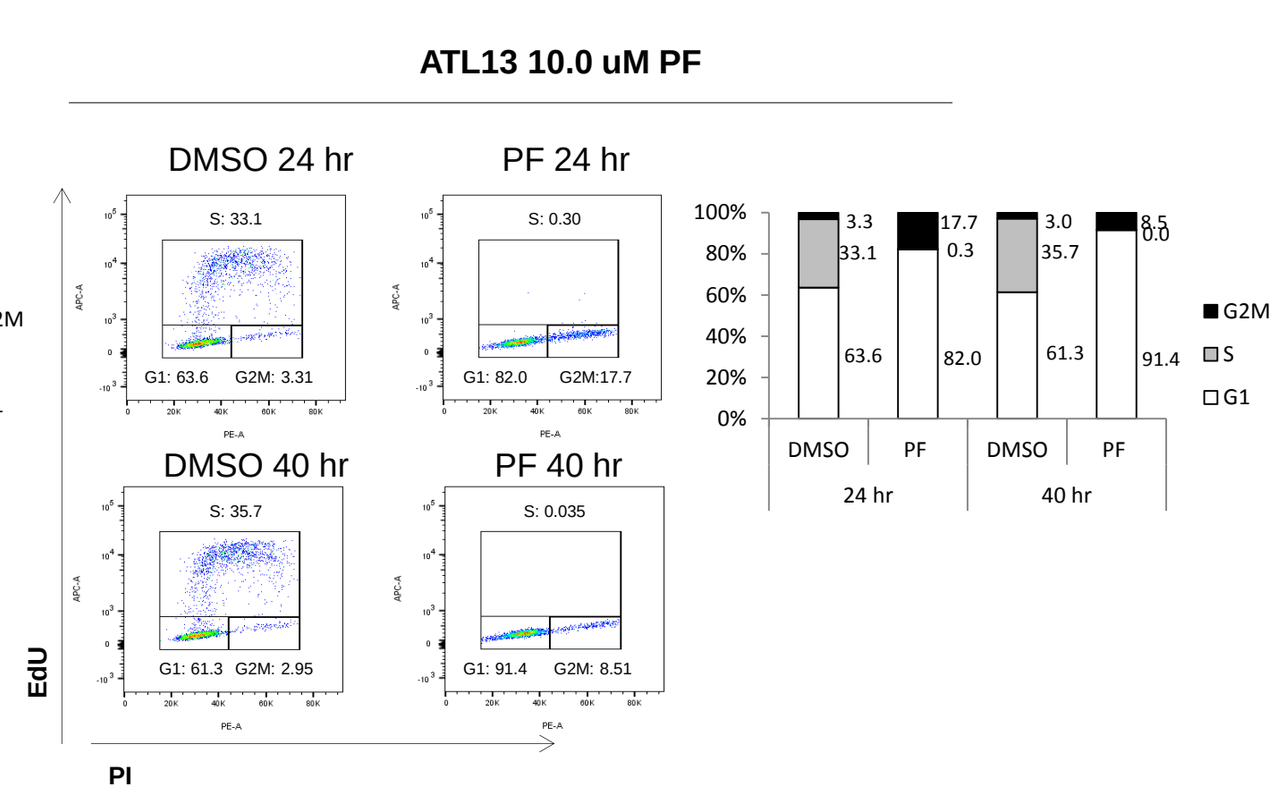

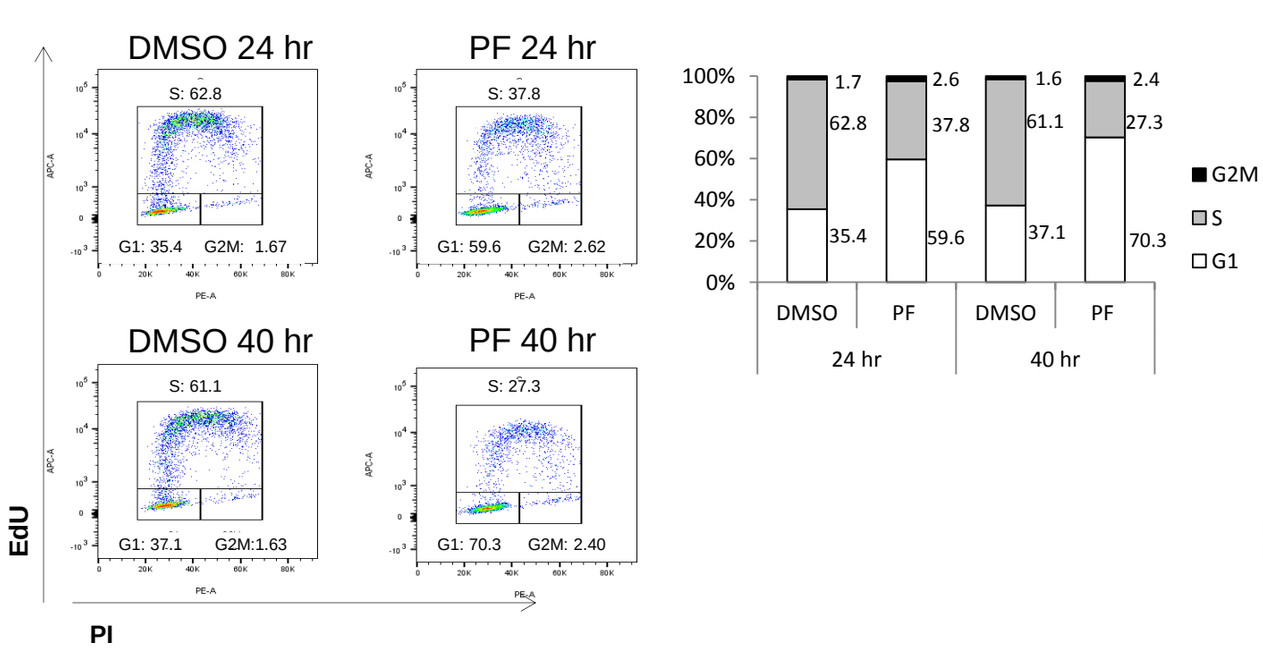

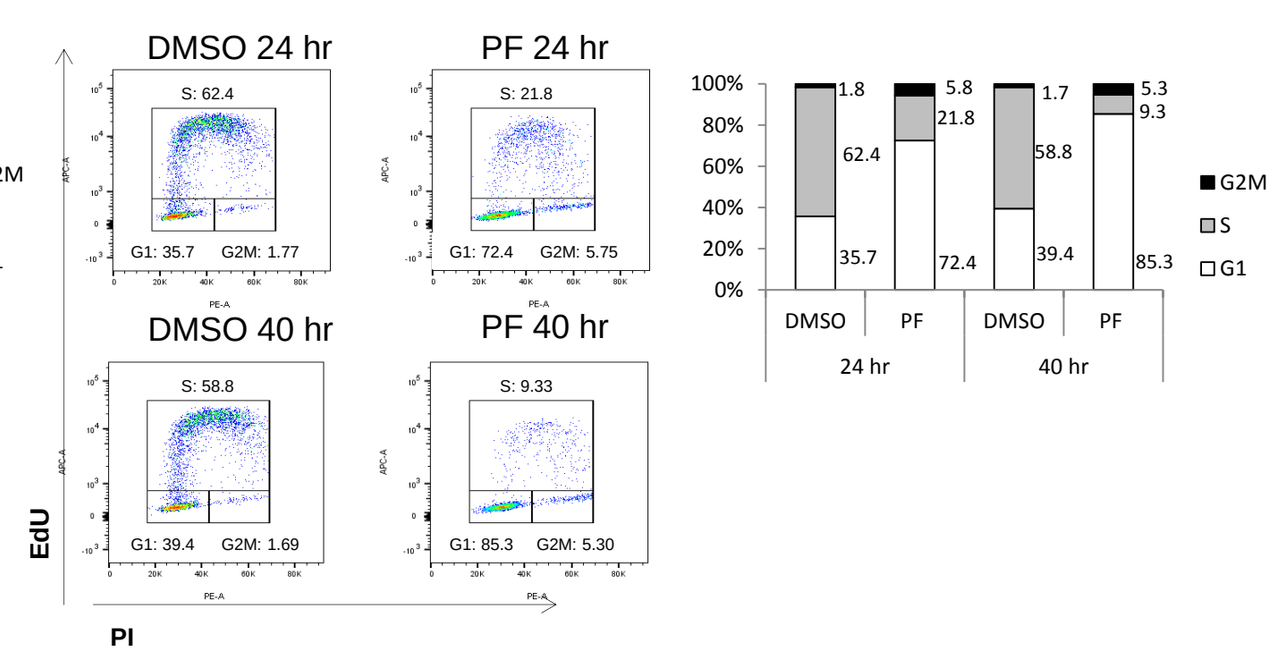

Figure S6 (Results are related to Figure 3B). Cell cycle analysis of 3 NA-ATLL cell lines treated with PF for 24 and 40 hours. Cell cultures were treated with indicated concentration of PF for 24 and 48 hours followed by cell cycle analysis based on EdU/PI staining. Shown are flow cytometry plots and bar graphs according to the percentage of cells in the G1, S, and G2/M gates.

Chung et al., Figure S6

Figure S7. Changes in the expression of apoptosis and cell survival regulators 48 hours post PF treatment.

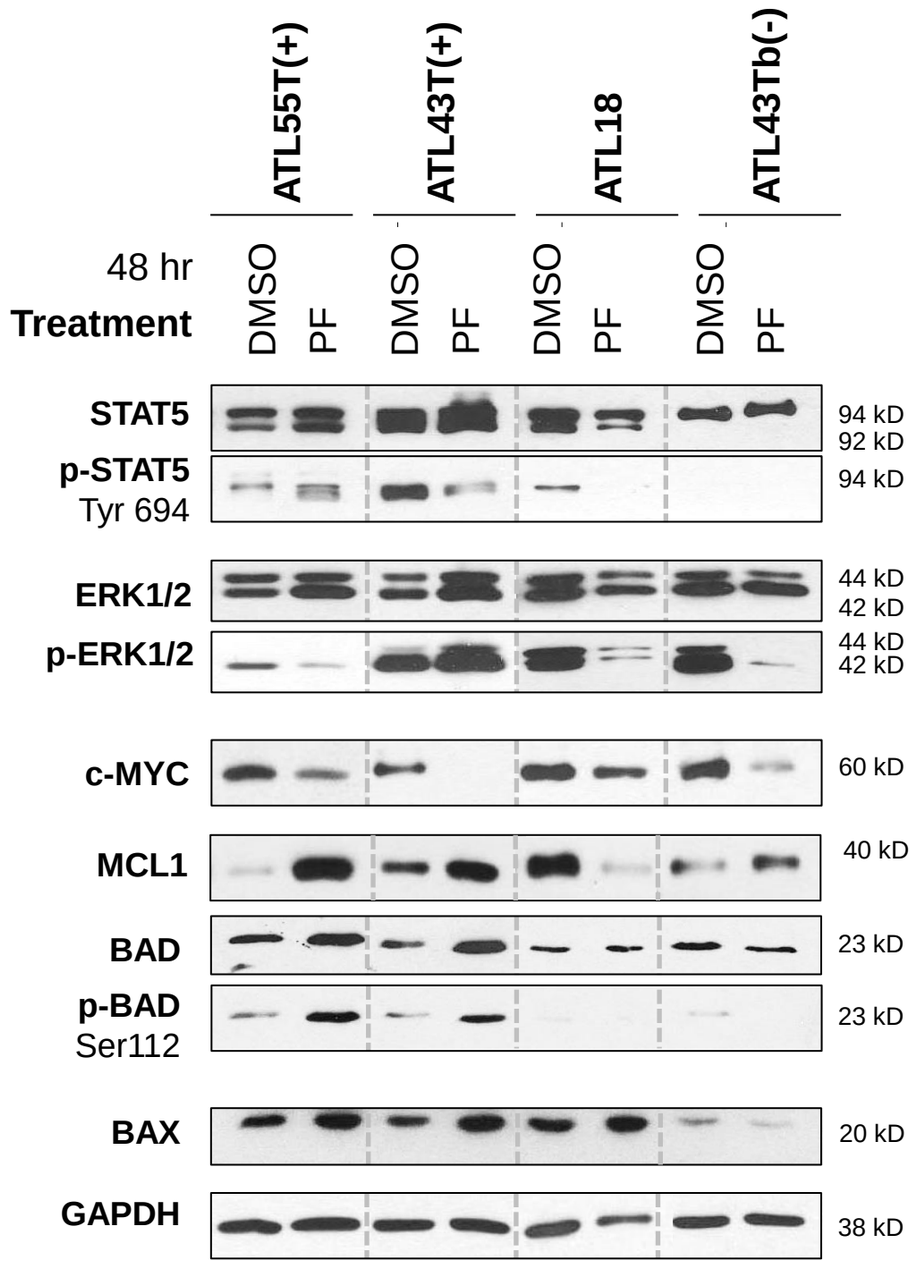

Figure S7 (Results are related to Figure 3C). Changes in protein expression of apoptosis and cell survival regulators 48 hours post PF treatment. Japanese ATLL cell cultures, ATL55T(+), ATL43T(+) and ATL43Tb(-), and North American ATLL cell culture, ATL18, were treated with PF at 2.5 and 2.0uM respectively for 48 hours. Cells were harvested post treatment for whole cell protein lysates and immunoblotted for markers indicated.

Figure S8. Roles of CADM1, PAK1, and PAK2 in cell adhesion to the HK feeder.

A

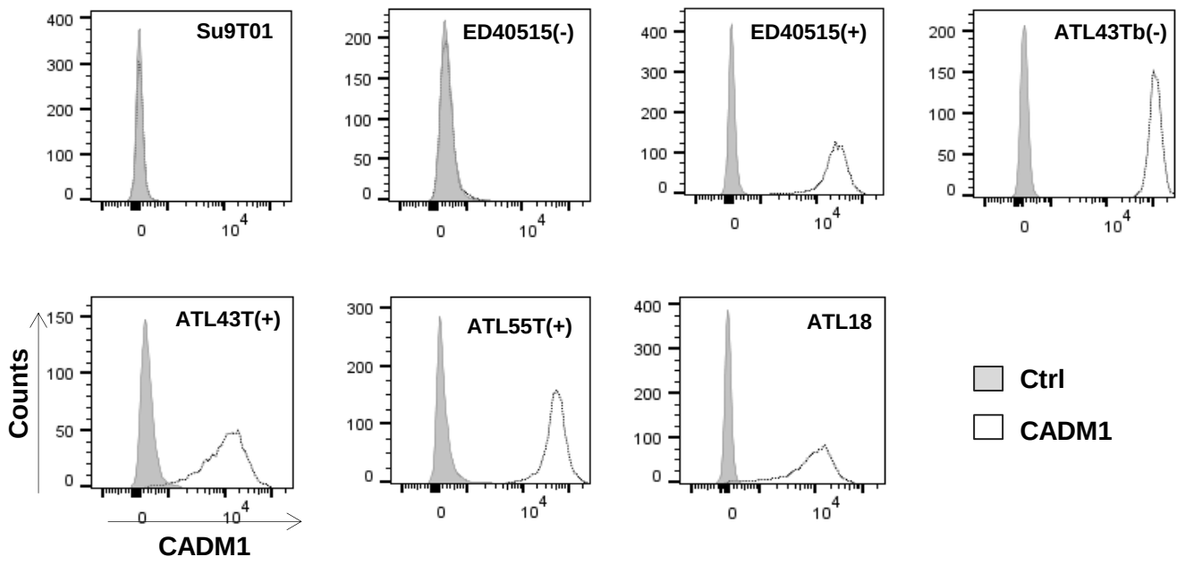

C

ATLL cultures	CADM1 expression	Adherence to HK	Interference by PF
Su9T01	-	-	-
ED40515(-)	-	-	-
ED40515(+)	+	+	+
ATL43Tb(-)	+	+	+
ATL43T(+)	+	+	+
ATL55T(+)	+	+	+
ATL18	+	+	+

B

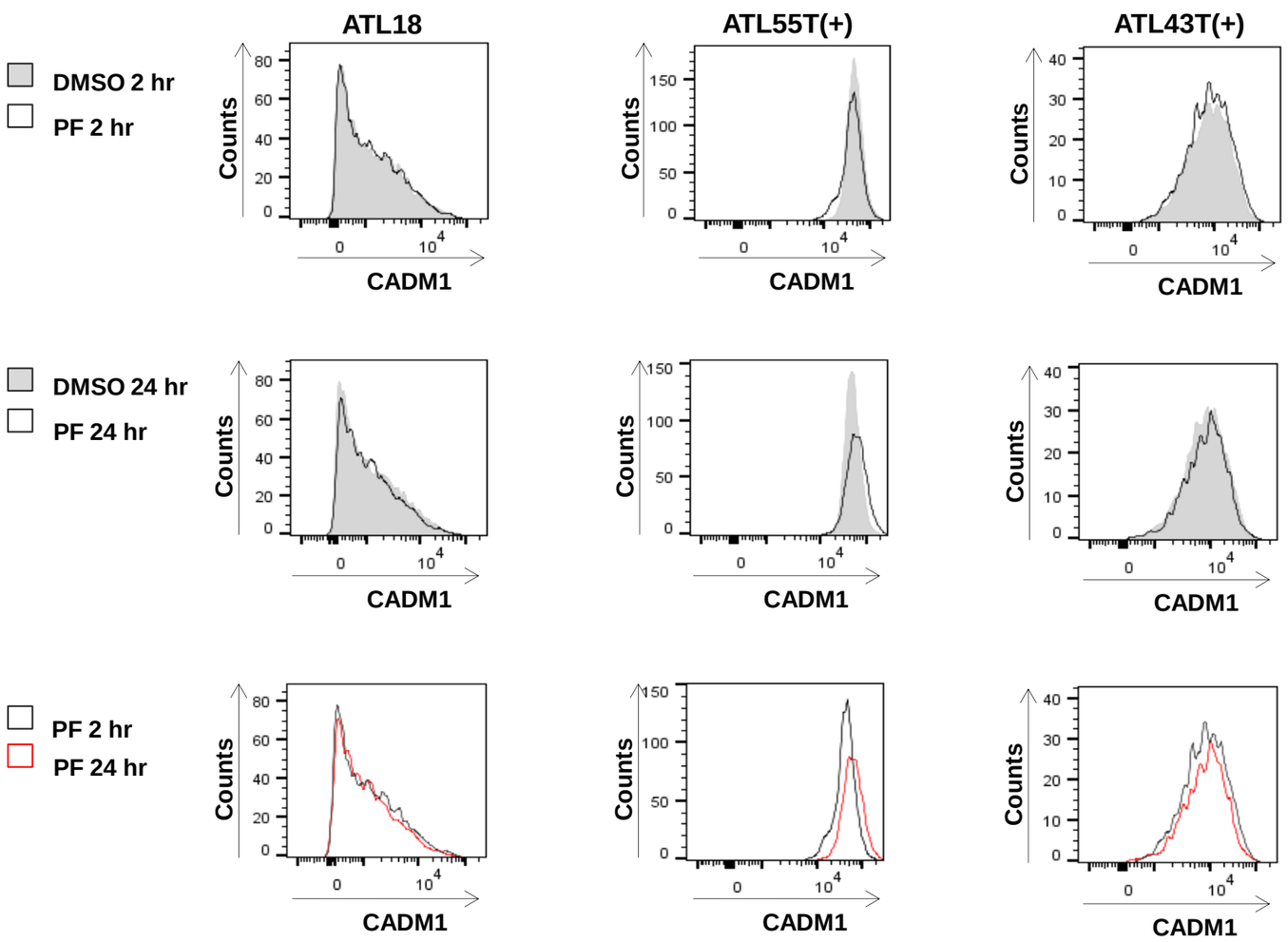

D

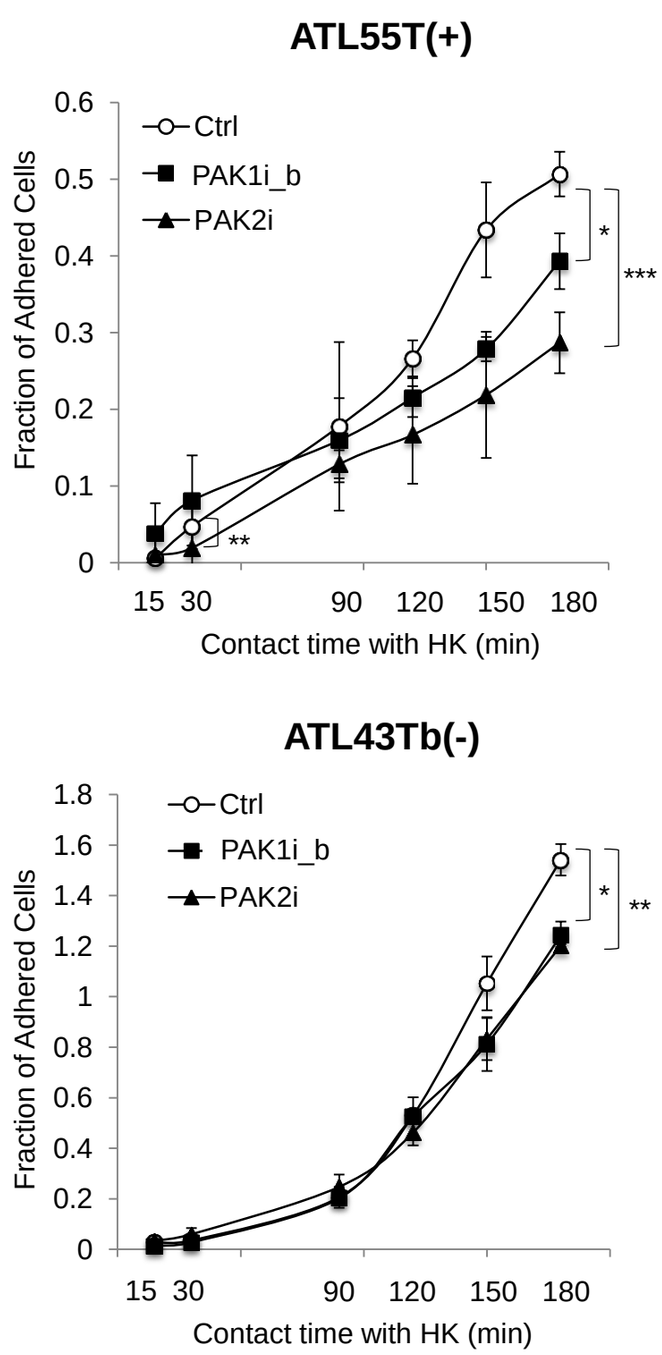

Figure S8 (Results are related to Figure 4). Roles of CADM1, PAK1, and PAK2 in cell adhesion to the HK feeder.
(A) Baseline CADM1 expression pattern based on flow cytometry analysis.
(B) CADM1 expression is not altered by short-term PF treatment. Three ATLL cell lines, ATL18, ATL55T(+), and ATL43T(+), were treated with 2 to 2.5 uM PF 2 (top row) and 24 hours (middle row) followed by flow cytometry analysis for CADM1 expression. Sytox Green (SG) nucleic acid stain was used to mark live (SG-) versus dead (SG+) cell fractions. Histograms represents live cell populations (SG-) that are stained positive for CADM1 on the cell surface. Bottom row is the overlay of the CADM1 histograms from 2 and 24 hours post PF treatment.
(C) Summary of CADM1 expression status, HK binding capability, and the impact of PAK inhibition on HK adherence.
(D) Impact of siRNA-mediated PAK1 or PAK2 KD on binding of ATLL cells to the HK feeder was measured 48 hours after siRNA transfection in a 3 hour time course as described in Figure 4C. Results shown are representative of at least 2 independent experiments

Figure S9. Apoptosis and cell cycle analysis of ATL55T(+) and ATL43Tb(-) cells following siRNA mediated PAK1 and PAK2 knock-down

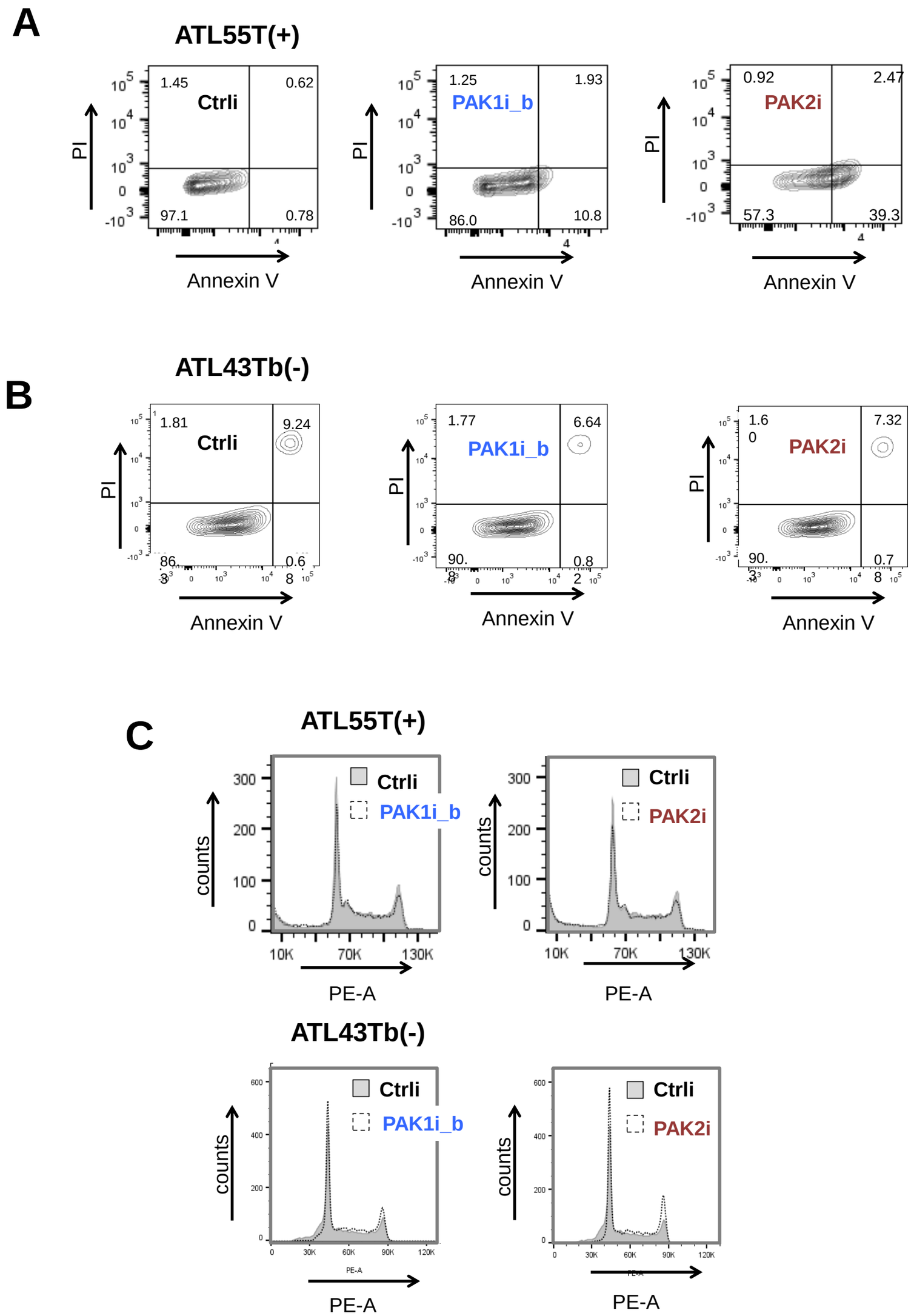

Figure S9 (Results are related to Figure 5). Apoptosis and cell cycle analysis of ATL55T(+) and ATL43Tb(-) cells following siRNA mediated PAK1 and PAK2 knock-down.

ATL55T(+) and ATL43Tb(-) cells were electroporated with siRNA targeting PAK1 or PAK2 at 100uM concentration. Cells were harvested 72 hours post electroporation for apoptosis (**A-B**) and cell cycle (**C**) analysis based on AV/PI and PI staining, respectively.

Figure S10. Changes in proliferation and survival regulators in ATL43Tb(-) cells following PAK1 or PAK2 knock-down

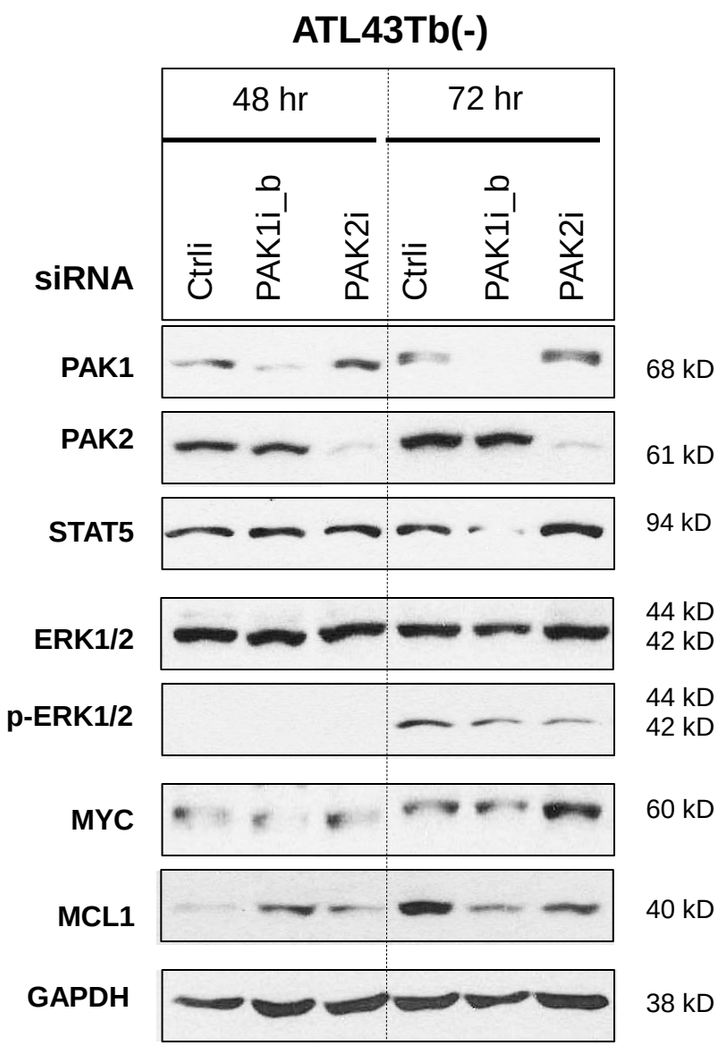

Figure S10 (Results are related to Figure 5). Proliferation and survival factors in ATL43Tb(-) cells upon siRNA mediated-knockdown of PAK1 or PAK2. ATL43Tb(-) cells were electroporated with siRNA targeting PAK1 or PAK2 at 100uM concentration. Cells were harvested 48 and 72 hours post electroporation for whole cell protein lysates and immunoblotted with markers indicated. Note: In ATL43Tb(-) cells, total STAT5 is expressed but no STAT5 phosphorylation at tyrosine 694 is detected.

Figure S11. PF response in CDX and PDX-derived xenograft models

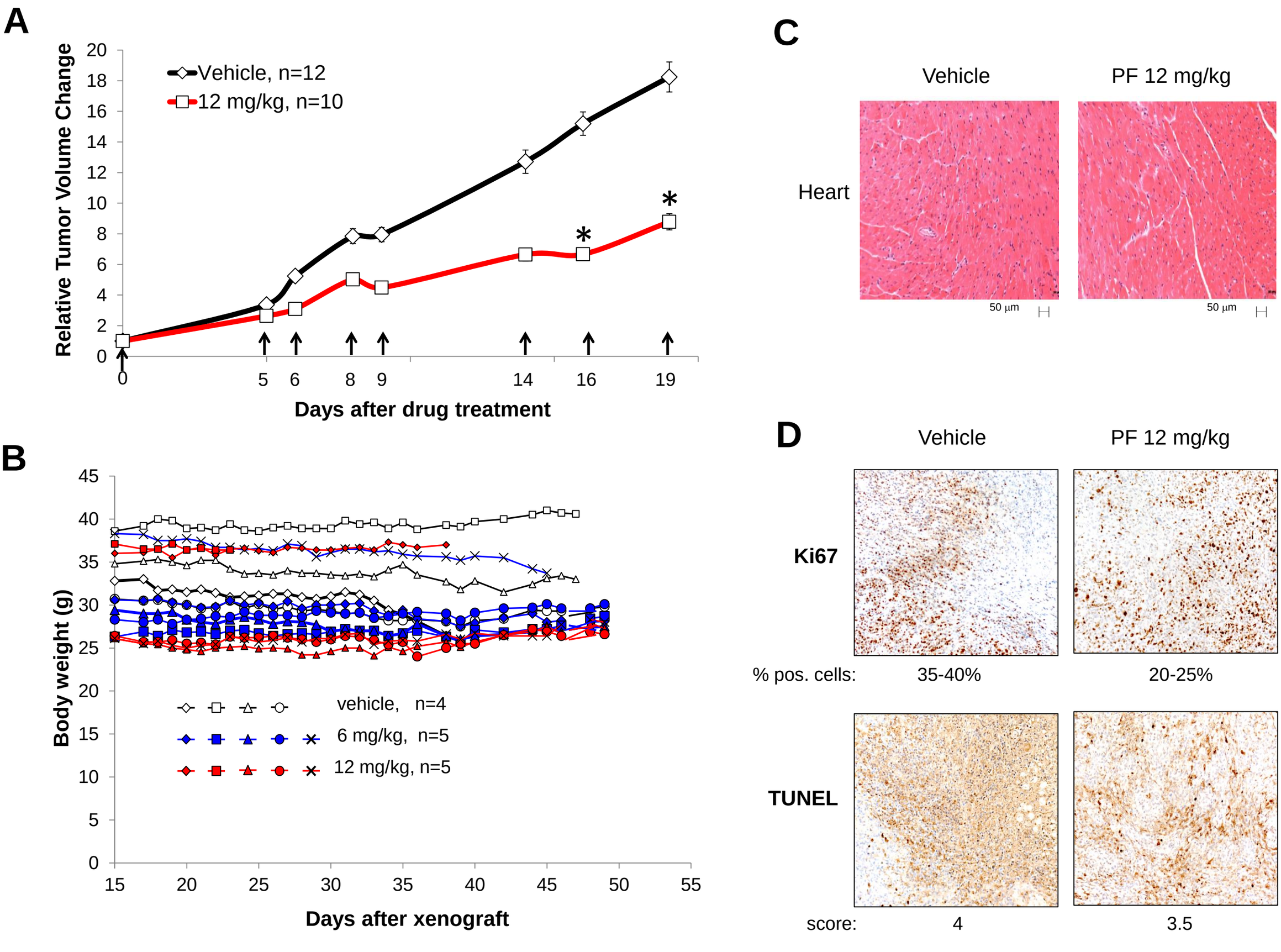

Figure S11 (Results are related to Figure 6). Additional data on the effects of PF treatment in the CDX (A) and PDX-derived xenograft (B-D) models.

(A) tumor weight of NGS mice bearing subcutaneous tumor mass derived form ATL43Tb(-) cells. Mice were randomly assigned to 2 treatment arms: vehicle control (n = 12) and PF 12 mg/kg (n = 10) (*i.p*. doses were given on days denoted with the arrow). Results presented are mean tumor volumes with error bars indicating standard error of the mean. Compared with vehicle control, 12 mg/kg treatment showed significant activity on day 16 and day 19 post PF treatment ($P < 0.05$, 2-tailed Student t test).

(B) Body weight of NGS mice treated with PF or veichle. Mice were randomly assigned to 3 treatment arms: vehicle control (n = 4), PF 6 mg/kg (n = 5), and PF 12 mg/kg (n = 5).

(C) Grossly normal histology of the heart in vehicle, and NGS mice bearing 19 days post treatment.

(D) IHC-based evaluation of cell proliferation (Ki67) and apoptosis (TUNEL) in vehicle- and 12 mg/kg PF-treated subcutaneous tumor mass. Ki67 is evaluated as a proliferation index (approximate % of positively stained cells) while TUNEL staining is scored semi-quantitatively as: --, no positive staining; 1, minimal positive staining; 2, mild positive staining; 3, moderate positive staining; 4, marked positive staining; 5, diffuse positive staining.

Supplementary Table S1

List of antibodies used for Western blot and flow cytometry

Antibodies for Western blot	Company	Catalog number	Dilution
PAK1	Cell Signaling Technology	2602	1 : 10,000
PAK2	Cell Signaling Technology	2615	1 : 10,000
PAK4	Cell Signaling Technology	3242	1 : 10,000
Phospho-PAK1 (Ser144)/PAK2(Ser141)	Cell Signaling Technology	2606	1 : 1,000
Phospho-PAK1 (Ser199/204)/PAK2(Ser192/197)	Cell Signaling Technology	2605	1 : 1,000
Phospho-PAK1 (Thr423)/PAK2(Thr402)	Cell Signaling Technology	2601	1 : 1,000
Phospho-PAK2 (Ser20)	Cell Signaling Technology	2607	1 : 1,000
Phospho-PAK4 (Ser474)/PAK5 (Ser602)/PAK6(Ser560)	Cell Signaling Technology	3241	1 : 1,000
STAT5	Cell Signaling Technology	9363	1 : 10,000
phospho-STAT5 (Tyr694)	Cell Signaling Technology	9351	1 : 1,000
ERK	Cell Signaling Technology	9102	1 : 10,000
phospho-ERK (Thr202)/(Tyr204)	Cell Signaling Technology	9101	1 : 1,000
MYC	Santa Cruz Biotechnology	sc-33	1 : 1,000
MCL1	Santa Cruz Biotechnology	sc-819	1 : 1,000
BAX	Cell Signaling Technology	2772	1 : 1,000
BAD	Cell Signaling Technology	9292	1 : 1,000
phospho-BAD (Ser112)	Cell Signaling Technology	5284	1 : 1,000
Cyclin B1	Santa Cruz Biotechnology	sc-595	1 : 1,000
Phospho-Histone H3 (Ser10)	Cell Signaling Technology	53348	1 : 1,000
GAPDH	Santa Cruz Biotechnology	sc-25778	1 : 10,000

Antibodies for Flow Cytometry	Company	Catalog number	Usage
Anti-SynCAM(TSLC1/CADM1) Alexa Fluor 647	MBL	CM004-A64	1 ug/test
FITC Annexin V	BD Pharmingen	556419	5 ul/test
Anti-CD45 Alexa Fluor 700	Biolegend	304024	1 ug/test

Supplementary Table S2

Primers for qPCR

Primers	Sequence
human PAK1 Forward	CAACTCGGGACGTGGCTAC
human PAK1 Reverse	CAGTATTCCGGGTCAAAGCAT
human PAK2 Forward	CACCCGCAGTAGTGACAGAG
human PAK2 Reverse	GGGTCAATTACAGACCGTGTG
human PAK3 Forward	CCAGGCTTCGCTCTATCTTCC
human PAK3 Reverse	TCAAACCCCACATGAATCGTATG
human PAK4 Forward	GGACATCAAGAGCGACTCGAT
human PAK4 Reverse	CGACCAGCGACTTCCTTCG
human PAK5 Forward	CCAAAGCCTATGGTGGACCC
human PAK5 Reverse	AGGCCGTTGATGGAGGTTTC
human PAK6 Forward	ACCAGCACTTCAACGTGGTG
human PAK6 Reverse	GACTTGGGAGACGATGTCTGT
human HPRT1 Forward	TGACACTGGCAAAACAATGCA
human HPRT1 Reverse	GGTCCTTTTCACCAGCAAGCT
human ACTB Forward	CTGGAACGGTGAAGGTGACA
human ACTB Reverse	AAGGGACTTCCTGTAACAATGCA
human HMBS Forward	GGCAATGCGGCTGCAA
human HMBS Reverse	GGGTACCCACGCGAATCAC
human HBZ Forward	CAGTAGGGCGTGACGATGTA
Human HBZ Reverse	CAAGGATAATAGCCCGTCCA
Human TAX Forward	CGGATACCCAGTCTACGTGTT
Human TAX Reverse	CAGTAGGGCGTGACGATGTA